

Studying Hydrodynamics Behaviour in a Fluidized Bed

by

Luqman Hakim B. Hassan

Dissertation submitted in partial fulfillment of
the requirements for the
Bachelor of Engineering (Hons)
(Chemical Engineering)

SEPTEMBER 2011

Universiti Teknologi PETRONAS
Bandar Seri Iskandar
31750 Tronoh
Perak Darul Ridzuan

CERTIFICATION OF APPROVAL

Studying Hydrodynamics Behaviour in a Fluidized Bed

by

Luqman Hakim B. Hassan

A project dissertation submitted to the
Chemical Engineering Programme
Universiti Teknologi PETRONAS
in partial fulfillment of the requirement for the
BACHELOR OF ENGINEERING (Hons)
(CHEMICAL ENGINEERING)

Approved by,



(Name of Main Supervisor)
Dr. Ku Zilati Ku Shaari
Senior Lecturer
Chemical Engineering Department
Universiti Teknologi PETRONAS

UNIVERSITI TEKNOLOGI PETRONAS

TRONOH, PERAK

September 2011

CERTIFICATION OF ORIGINALITY

This is to certify that I am responsible for the work submitted in this project, that the original work is my own except as specified in the references and acknowledgements, and that the original work contained herein have not been undertaken or done by unspecified sources or persons.



LUQMAN HAKIM BIN HASSAN

ABSTRACT

An experimental investigation has been performed, studying hydrodynamics behaviour of two-dimensional bubbling in a gas-solid fluidized bed with a CCD high speed camera. The main focus for analysing on the influence of varies pressure and particle size towards the bubble diameter bubble density, bed expansion and bubble rising velocity.

A method has been implemented to verify that the image recording scheme yielded reproducible time-averaged flow patterns. The high speed camera with a speed up to 3,000 frames per second was placed in front of the rectangular column to observe the hydrodynamics behaviour. Image analysis software was used to analyse the image that allows determination of bubble characteristics.

Bubble diameter will increase with height above air distributor until it reaches maximum bubble height, h^* , beyond which bubbles do not grow further and become unstable and break up. The maximum bubble height, h^* is a minor effect on differential particle size and pressure. Bubble density increase with particle size at low pressure and decrease with particle size at high pressure. The bed expansion increases with pressure and decrease with particle size.

ACKNOWLEDGEMENT

In the name of Allah S.W.T. the most merciful and compassionate, praise to Allah, he is the Almighty, eternal blessing and peace upon the Glory of the Universe, our beloved Prophet Muhammad (S.A.W.), and his family and companions.

The special thank goes to my helpful supervisor, Dr. Ku Zilati Ku Shaari. The supervision and support that she gave truly help the progression and smoothness of the project. The co-operation is much indeed appreciated.

My grateful thanks also go to both Mr. Khairul Anwar Bin Hj Ahmad and Mr. Mohd Fahmi Bin Ahmad Razali big contribution and hard worked from both of them during my 3 weeks using high-speed camera at Block 15 (Mechanical Engineering Department) is very great indeed. The project would be nothing without the help and explanation from both of you.

Great deals appreciated go to the contribution of my department - Department of Chemical Engineering. I am also would like to thankful the Coordinator of Final Year Project - Dr. Lukman Ismail.

Furthermore, Mr Fazli Zainal and Mr Firdaus, the technicians in the Department of Chemical Engineering laboratory that patient in helping me complete this program. Not to forget Dr. Dr Lau Kok Keong for the kindness to let me use his fluidized bed.

Last but not least I would like to thank my friends especially those who work together as colleagues under Dr Ku Zilati Ku Shaari – Miss Yon Norasyikin Samsudin and Miss Norliza Mat Sidik for the wise ideas throughout the project.

TABLE OF CONTENTS

CERTIFICATION	II
ABSTRACT	IV
CHAPTER 1: INTRODUCTION	1
CHAPTER 2: LITERATURE REVIEW	6
CHAPTER 3: METHODOLOGY	9
CHAPTER 4: RESULTS AND DISCUSSIONS	18
CHAPTER 5: CONCLUSIONS AND RECOMMENDATIONS	41
REFERENCES	44
APPENDICES	47

Appendix I

Appendix II

Appendix III

Appendix IV

Appendix V

LIST OF FIGURES

Figure 1.1: (a) Fixed bed state (b) Expanded bed at minimum fluidization gas velocity (c) Bubbling fluidized bed (d) Slugging regime (e) Entrainment of particles	2
Figure 1.2: (a) Fixed bed state (b) Expanded bed at minimum fluidization gas velocity (c) Bubbling fluidized bed (d) Slugging regime (e) Entrainment of particles	3
Figure 3.1: Fluidized bed equipments.	9
Figure 3.2: Camera setup used in the video imaging of the tablet movement through the rectangular column	11
Figure 3.3: Experimental setup of the fluidization system	12
Figure 3.4: Principle of digital image analysis for a bubbling fluidized bed (a) original image (b) binary image	14
Figure 3.5: Bubble diameter measurement technique	15
Figure 3.6: Data for bubble density	15
Figure 3.7: Bed expansion measurement technique	16
Figure 3.8: Height at Early point (0024) for $D_p = 1.64\text{mm}$, 0.25bar	17
Figure 3.9: Height at End point (0076) for $D_p = 1.64\text{mm}$, 0.25bar	17
Figure 4.1: Bubble diameter versus height above air distributor for $D_p = 1.64\text{mm}$, $H=80\text{mm}$	21

Figure 4.2: Bubble diameter versus height above air distributor for $D_p = 2.36\text{mm}$, $H_{mf}=80\text{mm}$	21
Figure 4.3: Bubble diameter versus height above air distributor for $D_p = 3.35\text{mm}$, $H_{mf}=80\text{mm}$	22
Figure 4.4: Bubble diameter versus height above air distributor for $D_p = 1.64\text{mm}$, $H_{mf}=80\text{mm}$, Pressure= 1.0bar	23
Figure 4.5: Bubble diameter versus height above air distributor, $D_p = 1.64\text{mm}$, $H_{mf}=80\text{mm}$, Pressure= 0.25-1.0bar	23
Figure 4.6: Bubble diameter versus height above air distributor for $D_p = 2.36\text{mm}$, $H_{mf}=80\text{mm}$, Pressure= 0.25bar	24
Figure 4.7: Bubble diameter versus height above air distributor for $D_p = 2.36\text{mm}$, $H_{mf}=80\text{mm}$, Pressure= 0.5bar	25
Figure 4.8: Bubble diameter versus height above air distributor for $D_p = 2.36\text{mm}$, $H_{mf}=80\text{mm}$, Pressure= 0.75bar	25
Figure 4.9: Bubble diameter versus height above air distributor for $D_p = 2.36\text{mm}$, $H_{mf}=80\text{mm}$, Pressure= 1.0bar	26
Figure 4.10: Bubble diameter versus height above air distributor for $D_p = 2.36\text{mm}$, $H_{mf}=80\text{mm}$, Pressure= 0.25-1.0bar	27
Figure 4.11: Bubble diameter versus height above air distributor for $D_p = 3.35\text{mm}$, $H_{mf}=80\text{mm}$, Pressure= 0.25bar	28
Figure 4.12: Bubble diameter versus height above air distributor for $D_p = 3.35\text{mm}$, $H_{mf}=80\text{mm}$, Pressure= 0.5bar	28
Figure 4.13: Bubble diameter versus height above air distributor for $D_p = 3.35\text{mm}$, $H_{mf}=80\text{mm}$, Pressure= 0.75bar	29

Figure 4.14: Bubble diameter versus height above air distributor for $D_p = 3.35\text{mm}$, $H_{mf}=80\text{mm}$, Pressure= 1.0bar	29
Figure 4.15: Bubble diameter versus height above air distributor for $D_p = 3.35\text{mm}$, $H_{mf}=80\text{mm}$, Pressure= 0.25-1.0bar	30
Figure 4.16: Bubble diameter versus height above air distributor for $D_p = 1.64, 2.36$ and 3.35mm , $H_{mf}=50\text{mm}$, Pressure= 0.25bar	31
Figure 4.17: Bubble diameter versus height above air distributor for $D_p = 1.64, 2.36$ and 3.35mm , $H_{mf}=50\text{mm}$, Pressure= 0.5bar	32
Figure 4.18: Bubble diameter versus height above air distributor for $D_p = 1.64, 2.36$ and 3.35mm , $H_{mf}=50\text{mm}$, Pressure= 0.75bar	32
Figure 4.19: Bubble diameter versus height above air distributor for $D_p = 1.64, 2.36$ and 3.35mm , $H_{mf}=50\text{mm}$, Pressure= 1.0bar	33
Figure 4.20: Bubble density versus pressure	34
Figure 4.21: Expanded bed height versus Pressure	36
Figure 4.22: Image of sand with the $D_p= 1.64\text{mm}$, $H=80\text{mm}$, Pressure= 0.25 bar (a) source of air is unmoved (b) source of air moving like sprinkler system	43

LIST OF TABLES

Table 4.1: Bubble diameter distribution at specific height above air distributor for $D_p = 1.64\text{mm}$	18
Table 4.2: Bubble diameter distribution at specific height above air distributor for $D_p = 2.36\text{mm}$	19
Table 4.3: Bubble diameter distribution at specific height above air distributor for $D_p = 3.35\text{mm}$	20
Table 4.4: Bubble density for $D_p = 1.64\text{mm}$	33
Table 4.5: Bubble density for $D_p = 2.36\text{mm}$	34
Table 4.6: Bubble density for $D_p = 3.35\text{mm}$	34
Table 4.7: Bed expansion for $D_p = 1.64\text{mm}$	25
Table 4.8: Bed expansion for $D_p = 2.36\text{mm}$	36
Table 4.9: Bed expansion for $D_p = 3.35\text{mm}$	36
Table 4.10: Velocity for $D_p = 1.64\text{mm}$, 0.25bar	37
Table 4.11: Velocity for $D_p = 1.64\text{mm}$, 0.5 bar	38
Table 4.12: Velocity for $D_p = 1.64\text{mm}$, 0.75 bar	38
Table 4.13: Velocity for $D_p = 1.64\text{mm}$, 1.0 bar	39

CHAPTER 1

INTRODUCTION

1.1 BACKGROUND OF STUDY

According to I. Roghair, 2007, fluidization is a phenomenon of transforming fixed bed particles which has static behavior, to a dynamic state. This is done with an upward fluid flow through the bed. In industry, fluidization is performed in Fluidized Bed Reactor (FBR). These are used in a wide field, e.g. for the polymerization of olefins, drying of starch and combustion of coal, but even the cinema popcorn machine uses the principle of fluidization. A particle system in fluidized behaves like a liquid. For example, the surface remains horizontally when the bed is tilted, and the objects with a higher density than that of the bed sink into the bed.

When trying to describe the operation of a fluidized bed, Wurster Fluid Bed is being chosen as the best reference. The process starts when inlet air pushes the uncoated powder particles through the path of the fine mist that is released from the spray nozzle in the Wurster column. The coated particle travels up the Wurster column into an expansion chamber where it loses acceleration and starts to move outward towards the wall of the column. Powder particles reach their peak and fall to the bottom, are drawn into the underside of the column, repeating the bottom spray cycle. A schematic of Wurster Fluid Bed processing is shown in Figure 1.1

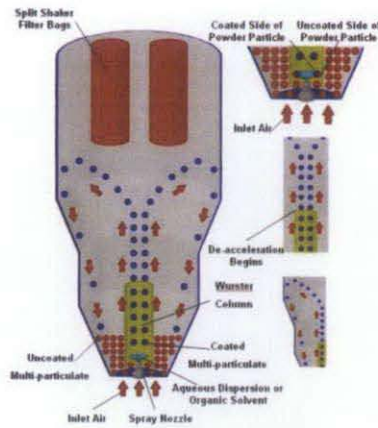


Figure 1.1: Schematic diagram of Wurster Fluid Bed processing.

(<http://www.mendelco.com/FluidBedProcessing.asp>, n.d)

Fluidized bed reactors show an excellent mass and heat transfer due to rapid mixing of the particles. Therefore, it is often used in large scale operations. Moreover, it responds slowly to changes in temperature and provides an excellent gas-solid contact.

The disadvantages of the fluidized bed are no uniform particle residence time, erosion of the vessel and internals due to the solid phase and a low gas conversion rate. In this project, gas-solid fluidization is considered. Gas is distributed over the column in which the particle bed is present. Although depending on the process, this is normally done by a bottom plate with gas inlets distributed over the surface of the distributor. The particles experience a drag force induced by the gas flow.

At low gas flow rates, the gas flows through the interstitial volume between the particles as packed bed state, Fig. 1.2 (a). Increasing the superficial gas velocity makes the particles to move further apart; the bed expands as the voidage between the particles grows larger. Bed expansion continues until the gas flow rate reaches a certain value. When the gravitational force equals the drag force of the gas on the particles, particles start to float as in Fig 1.2 (b). This gas flow rate is called the minimum fluidization gas velocity, u_{mf} .

At gas flow rates above umf , bubbles start to form above the distributor as shown in Fig. 1.2 (c). The bubbles rise through the particle phase due to the buoyancy force. Bubbles grow larger while rising due to gas entrainment and coalescence. Depending on the particle classification, bubbles may also break-up. The existence of bubbles in a fluidized bed causes mixing of the particles. The bubbles induce a stirring action and convective particle transport through the bed.

Different forms of fluidization are known. Increasing the gas flow beyond minimum fluidization velocity may results a bubbling fluidized bed. However, the column size causes the bubbles to be restricted by the walls; another regime is reached, called slugging as in Fig. 1.2 (d). The wide bubbles reach almost from wall to wall, while particles mainly rain down the wide bubbles. Entrainment of particles by the gas flow is shown in Fig. 1.2 (e). This work investigates the bubbling fluidization regime.

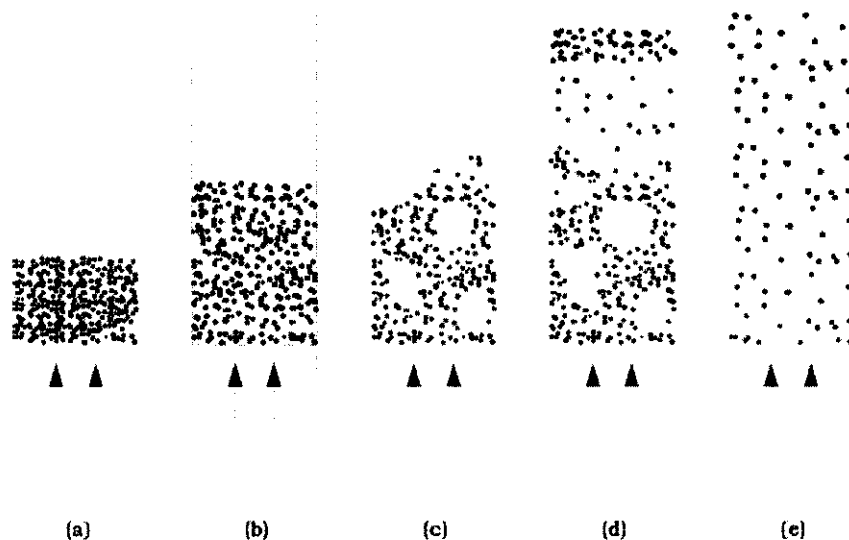


Figure 1.2: (a) Fixed bed state (b) Expanded bed at minimum fluidization gas velocity (c) Bubbling fluidized bed (d) Slugging regime (e) Entrainment of particles (I. Roghair, 2007)

1.2 PROBLEM STATEMENT

Gas-solid fluidized beds are widely employed in the chemical industry. Fluidized beds are often operated in a continuous way: particles are continuously added to and removed from the bed. In this way of operating a fluidized bed, the hydrodynamic behavior may be altered over time, due to either imposed or unwanted changes. Examples of imposed changes are changes in gas velocity or particle type. Examples of unwanted changes are often related to agglomeration or sintering of particles. (Ommen, 2001)

Moreover, fluidized beds are always been considering as unique, depend on many parameters such as pressure, volume, temperature, deflector, type of particle and etc. It is very difficult to do the study and achieve the main target; well distribution. To achieve well distribution throughout the process are favor by fluidized bed coating and combustion.

Furthermore, fluidized bed consists of a large mass of well-mixed particles: changes in particle properties are likely to be spread evenly over the complete bed and it may take a long time before they show up as drastic events such as de-fluidization. It is therefore worthwhile to have access to a method for detecting subtle changes in the fluidized bed hydrodynamics caused by small variations in particle properties before a catastrophic event such as de-fluidization takes place.

During the process, particle properties such as size change, leading to a change in the hydrodynamic behaviour of the fluidized bed over time. In such cases it is important to know when a certain desired final state is reached; a monitoring method for the hydrodynamics can give this information.

This project is performed in order to understand behavior of fluidized bed in different phenomena and operating parameters. Thus, the experiment will be performed to verify the hydrodynamics of the fluidized bed.

1.3 OBJECTIVES AND SCOPE OF STUDY

The objectives of this project are to study the influences of varies pressure and particle size on the

- i. bubble diameter
- ii. bubble density
- iii. bed expansion
- iv. bubble rising velocity

Scope of study:

- i. Conducting research on the fluidization related to the study.
- ii. Conducting experiments to determine the effect on different operating parameters to understand fluidization in rectangular column.

CHAPTER 2

LITERATURE REVIEW

2.1 FLUIDIZATION

Chemical processes based on the use of fluidized solids, although widely used on an industrial scale for some four decades, are currently increasing in importance as industry looks for improved methods for handling and reacting solid materials. (J.G, 2008). Moreover, the performance of fluidized bed coating is strongly influenced by the hydrodynamics of the fluidization process

2.1.1 Size of the particle in the fluidized bed

Shailendra, 2010, found bed voidage increases with the liquid velocity and depending in the particle size. It has been observed that the smaller particle size gains more velocity than the larger particles. Hence, bed voidage is a strong function of liquid velocity; it increases with the liquid velocity. The small particle size has more bed voidage than the larger particle size. In addition, it is easier to maintain fluidization quality with particles having a wide range that with particles of uniform size. In Tao Zhou, 1999 shows that the fluidized characteristics is greatly affected by the size of particles, and the smaller the size of particles, the bigger the inter-particle force, the worse the fluidized behaviour. Therefore with decreasing the size of particles, the required superficial gas velocity for fluidizing cohesive particles increases, and the bed pressure drop decreases, and the collapsing time is from long to short, and the elutriation increases. Moreover, particles naturally agglomerate to reduce the surface energy when the size of particles decreases to a certain value, such as several micrometers. Furthermore, the influence of extreme-sized particles in small proportions is insignificant according to D. Gauthier, 1999.

Study by Heinrich (2009) that develop a model to describe the particle size distribution and the seed formation for continuous external fluidized bed spray granulation. The related info that can be share is heat and mass transfer model. The following assumptions are;

- The fluidization of the fluidized bed is homogeneous, i.e. the porosity of the bed is constant
- Only the first period of drying is observed, i.e. the solid particles are non-hygroscopic and absorb no moisture.
- The liquid on the particles forms a coherent film of constant thickness Δf , which is independent of the particle diameter.
- Ideal plug-flow of the fluidization gas (PFTR model)
- Solid sizing is described by axial and radial dispersion coefficients.

2.1.2 Fluidizing velocity

Shaun (2003) had done the studies to examine the operating conditions (airflow rate and particle loading) and coater configuration (the gap between the draft tube and the air distributor) on solids motion. At a given airflow rate, large or heavy particles give a longer mean cycle time because smaller particles move more quickly in the draft tube for a given airflow rate and also pass more easily through the gap between the distributor and the draft tube. In a while, an increase in the airflow rate causes a decrease in the mean particle cycle time.

In the study by Subramaniam (2003), three main factors had been considered to be tested; fluidizing gas velocity, gap height and design of the tablet deflector. In term of air (gas) velocity, there is a significance effect even for the small range of particles tested. The variable with the supreme effect is the gap height. Two types of experiments can be run to evaluate the effect of tablet deflectors on coating variability within each bath; continuous-coating experiments and pulse-coating

experiments. From several type of deflectors been tested, one of the modified deflector has the highest coating efficiency and come out to turn out lowest dusting and tablet breakage.

CHAPTER 3

METHODOLOGY

3.1 PROCEDURE

The overall methodology of this study can be divided into two major parts:

- i. Experimental set-up
- ii. Image processing
- iii. Measuring technique

3.1.1 Experimental setup

The experiments described in this project are performed in a fluidized bed as shown in Fig. 3.1.

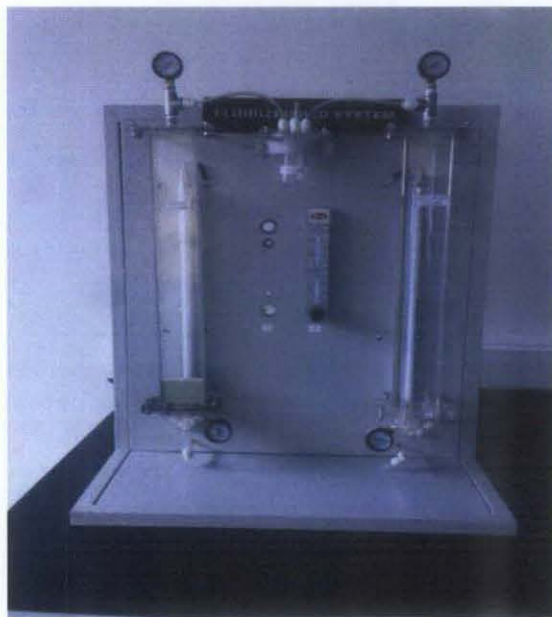


Figure 3.1: Fluidized bed equipments

It consists of a Plexiglass rectangular column with height of 55cm and width of 7cm, a syringe and air regulator that provides the fluidizing gas to establish required superficial gas velocity and camera Sony XC 75CE CCD, Sony Inc.

The distribution plate is made of a wire mesh tray with a pore size of 20 μm and a fractional free area of 60%. Sand and granular ureas with different size are used as the particle. The particles are sieved and particles are divided into 1.64mm(sand), 2.36mm(urea) and 3.35mm(urea). The gas-solid fluidization behaviour in the fluidized bed is investigated by changing pressure and particle sizes. The high speed camera is placed in front of the fluidized bed to capture the dynamic images at a speed of 3000 frames per second. The gas supply line is placed on the unmoving outer shell of the system. The fluidizing gas flows into the fluidized bed towards the bottom plate and fluidizes the particles by overcoming the centrifugal force. The high speed digital camera is placed above the system to capture the dynamic behaviour of the particle fluidization occurring in the fluidized bed at a speed of 3000 frames per second. Since the camera is fixed, the fluidization images can only be captured when the fluidized bed is in line with the lens during its moving. (Fei Wang, 2011)

The centre of a given tablet was then located in each field from the camera using a computer-generated crosshair. The horizontal and vertical distances between the successive images were computed and recorded. These data were then converted into magnitude and direction using the appropriate time lag. To obtain a map of tablet velocities in the rectangular column, the front face of the bed was divided into 8 cm by 7 cm square grids, and repeated measurements were made for each square.

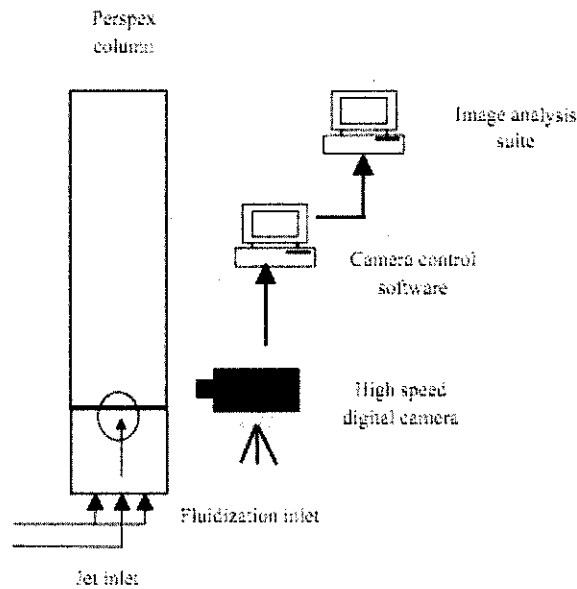


Figure 3.2: Camera setup used in the video imaging of the tablet movement through the rectangular column.

(Ganeshkumar Subramanian, 2003)

Voidage measurements were obtained in a given region of interest of the bed using a single CCD camera mounted perpendicular to the flat front face of the bed as in Fig.3.2. A shutter speed of 0.1 ms was used in order to obtain crisp, blur-free images. The software counted the number of tablets in the FOV automatically. To convert the number count to a voidage, the depth of field (DOF) of the camera and lens system had to be found. The DOF was obtained by calibration and using this value with the known volume of tablets in a given volume of bed, the local void volume in the bed was calculated. (Ganeshkumar Subramanian, 2003)

(Subramanian, 2003)

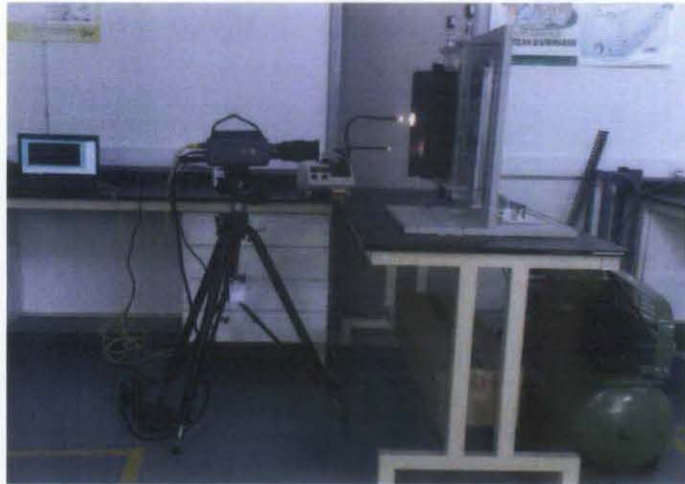


Figure 3.3: Experimental setup of the fluidization system.

All steps are repeated using different atomizing air pressure, different sizing of distribution plate and different granular urea size.

The results are compared and analyzed.

3.1.2 Image processing

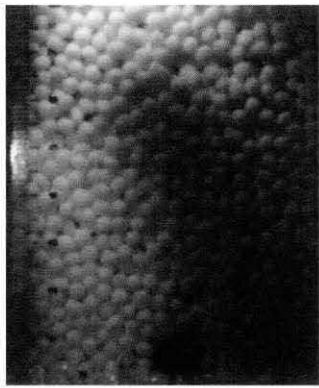
The image processing technique was follow as in Laihong Shen, 2004. The high shutter speed feature is essential for capturing fast moving images without a blurring effect, especially in the measurement of bubble movement. The auto-gain feature of digital video camera enables self-adjustment of the illumination level under the influence of the background or surrounding brightness. The films are recorded in the Red, Green and Blue (RGB) format. The time duration of each process is about 5-6 minutes. Then the films of digital video image from the video camera are transferred to a computer. The relative image area of the films is captured by an image frame-grabber. With the image processing toolbox of Matlab, computer software is developed to automate the procedures for image acquisition, data

processing and analysis for frame by frame. Then the time-averaged data about bubble characteristics in the bed is acquired.

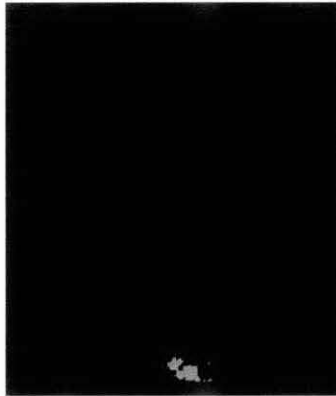
Fig. 3.4 is an example of image processing of a bubbling fluidized bed. It shows the process that bubbles grow up, split and erupt at the bed surface. The time delay between 1-2-3 frames is 1/3 second. Fig. 3.4 (a) is an original image. The image is then converted to the grey colour scheme. The initial step in image processing involves the discrimination of bubbles from the emulsion phase. When the image contrast is sufficient, phase identification is made possible by assigning a threshold value. With the process of image enhancement, data reduction, and analyzing images to extract information about their structure, the image is thresholded and then converted to the binary image. The binary segmentation mask of the bubbles is displayed in Fig. 3.4 (b). The white area in the bed is identified as bubble phase.

The threshold value has an impact on the detection of bubble boundaries. It is assessed through the comparison of a typical frame of the video film with the binary segmentation mask of bubbles. And then the value is chosen to be a universal threshold value, and be applied to the whole procedure of image processing. Image contrast of bubbling fluidized beds is normally high, the delineation of the bubble boundary with high accuracy is acquired. Thus the binary thresholded images are used to study the bubble characteristics in bubbling fluidized beds.

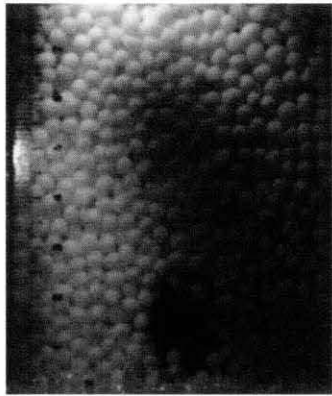
The detection and measurement of the bubble parameters are automated by employing a series of systematic edge searching routines. The initial step of the routine detects the number of the bubbles intersecting a line positioned at some height above the distributor. For every bubble detected, the complete boundary of the bubble may be delineated through further scanning across the image, as shown in Fig. 3.4 (b).



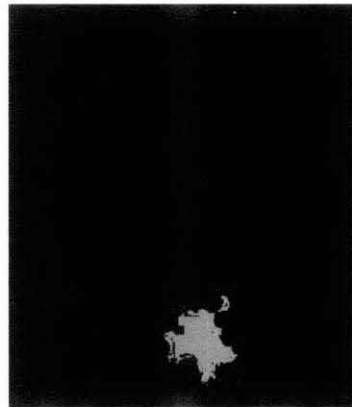
(a-1)



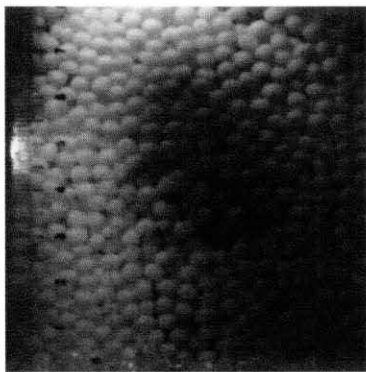
(b-1)



(a-2)



(b-2)



(a-3)



(b-3)

Figure 3.4: Principle of digital image analysis for a bubbling fluidized bed (a) original image (b) binary image

3.3 Measurement technique

3.3.1 Bubble diameter

Base on Fig.3.5, ruler is been put on the picture to measure what is the diameter bubble that been form. It will be measures at height above air distributor are 10, 20, 30, 40, 50, 60, 70 and 80mm.



Figure 3.5: Bubble diameter measurement technique

3.3.2 Bubble density

After the binary image had been produce as in Fig. 3.4(b), by using Image Analyzer CNET, the data as in Fig. 3.6 can be achieved.

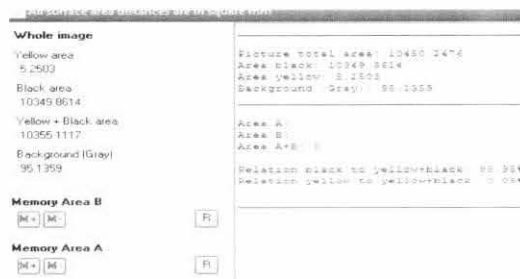


Figure 3.6: Data for bubble density

Bubble density can be inferred as follows:

$$\delta_b = \text{white projected area} / \text{specific area}$$
$$= \text{background (gray) area} / \text{total area}$$

3.3.3 Bed expansion

Based on Fig. 3.7, the new bed height will be determined after the gas flow has been supplied. The bed expansion is measured using a ruler by taking the highest location of the bed particle.

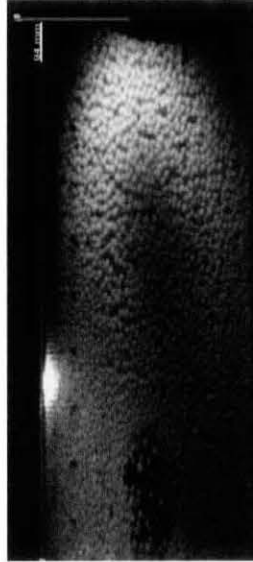


Figure 3.7: Bed expansion measurement technique

3.3.4 Velocity

Take a randomly frame and located certain particles as Early Point and been marking as 1st and 2nd as in Fig.3.8. Then, by manually observed the movement of the marking particles, a frame is selected and been considered as End Point as in Fig. 3.9.

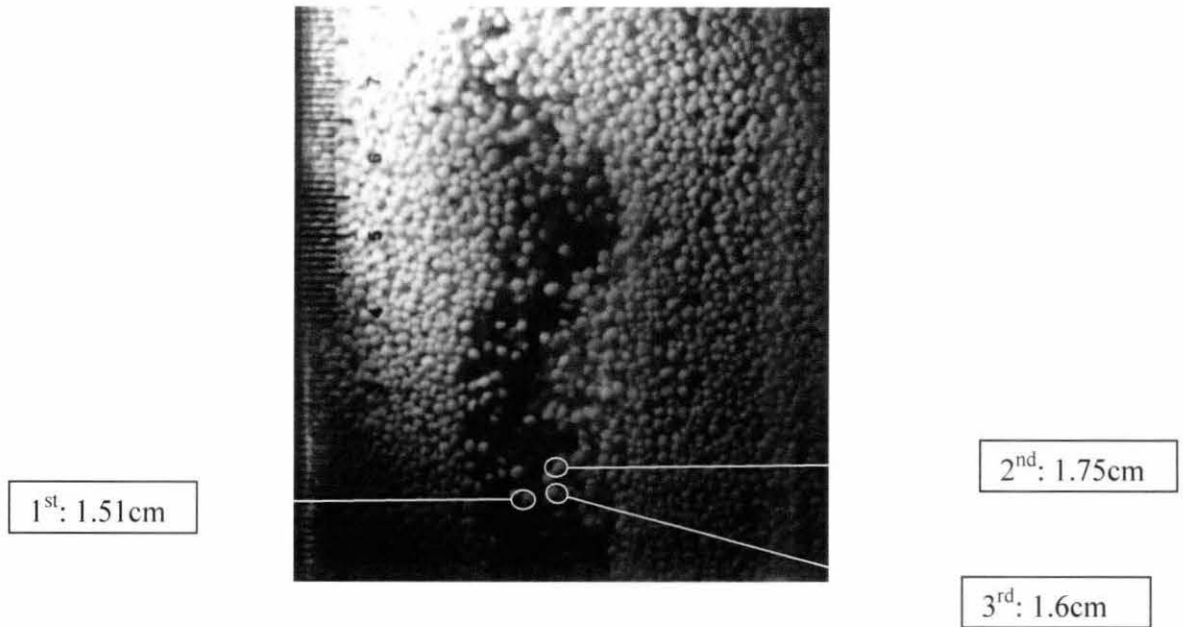


Figure 3.8: Height at Early point (0024) for $D_p = 1.64\text{mm}$, 0.25bar

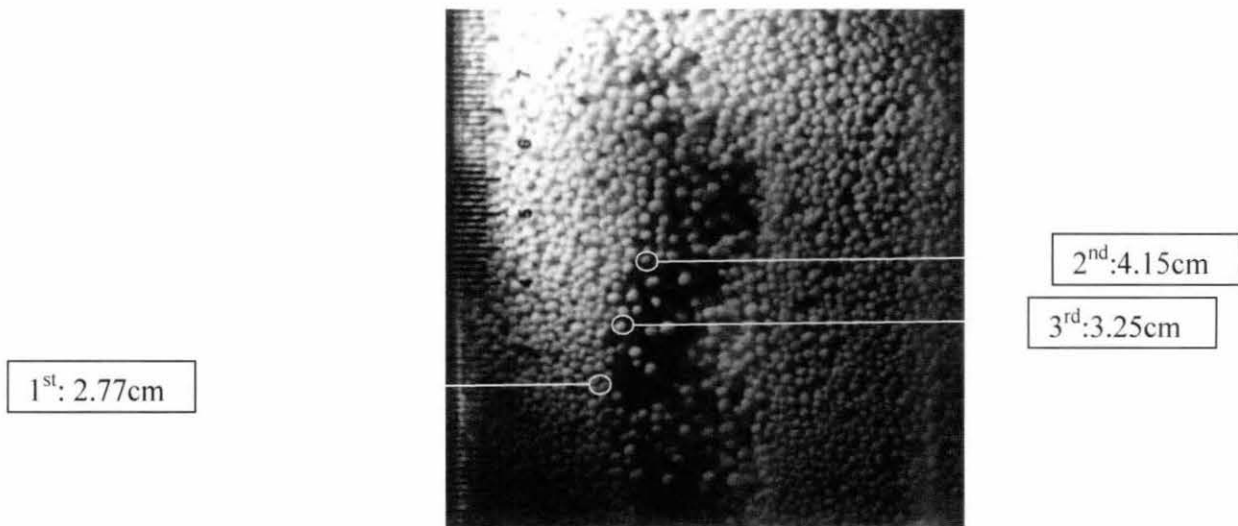


Figure 3.9: Height at End point (0076) for $D_p = 1.64\text{mm}$, 0.25bar

Example calculation of velocity is attached in Appendix I.

CHAPTER 4

RESULTS AND DISCUSSIONS

This chapter presents the findings and discussions from the results obtained during lab work of preparation of hydrodynamics behaviour in a fluidized bed. The experimental set up is as shown in Figure 3.3. Sand with the size of 1.64mm is being used as the reference as it is small particle. Sample urea with the size of 2.36mm and 3.35mm are the focusing particle for study. The result of hydrodynamics behaviour of sample urea with the size of 2.36mm and 3.35mm are being compared with sand that is already a common fluidized particle.

4.1 BUBBLE DIAMETER, D_b

Experimental data about bubble diameter distribution versus height above air distributor is calculated as in Appendix II. The results are show in Table 4.1, 4.2 and 4.3 for $D_p = 1.64\text{mm}$, $D_p = 2.36\text{mm}$ and $D_p = 3.35\text{mm}$, respectively.

Table 4.1: Bubble diameter distribution at specific height above air distributor for $D_p = 1.64\text{mm}$.

Pressure (bar)	Height (mm)	Bubble diameter (mm)
0.25	10	11.7
	20	14.7
0.5	10	9.8
	20	17
	30	22
	40	26.6
	50	34.4
	60	22
	70	10

0.75	10	8.8
	20	17
	30	20.5
	40	28.5
	50	36.4
	60	24.5
	70	10
	80	5
1	10	8.9
	20	13
	30	21.5
	40	30
	50	32.5
	60	25
	70	13.5
	80	10.9

Table 4.2: Bubble diameter distribution at specific height above air distributor for $D_p = 2.36\text{mm}$.

Pressure (bar)	Height (mm)	Bubble diameter (mm)
0.25	10	13.5
0.5	10	11
	20	17
	30	28.5
	40	30.5
	50	34
0.75	10	14
	20	20.5
	30	28.5
	40	32
	50	34

	60	35.5
	70	30.8125
	80	17
	10	15.5
	20	20
	30	24
	40	25
	50	29
	60	27
	70	27.8125
	80	35

Table 4.3: Bubble diameter distribution at specific height above air distributor for $D_p = 3.35\text{mm}$.

Pressure (bar)	Height (mm)	Bubble diameter (mm)
0.25	10	11.5
0.5	10	12
	20	14
0.75	10	9
	20	12
	30	16
	40	20
	50	18
	60	18.5
1	10	14.5
	20	19
	30	23
	40	27
	50	21
	60	7

4.1.1 Effect of pressure to the bubble diameter at certain height above air distributor

The graph of bubble diameter at certain height above air distributor of 0.25, 0.5, 0.75 and 1.0 bar for $D_p = 1.64\text{mm}$ are shown in Fig. 4.1, Fig. 4.2, Fig. 4.3 and 4.4.

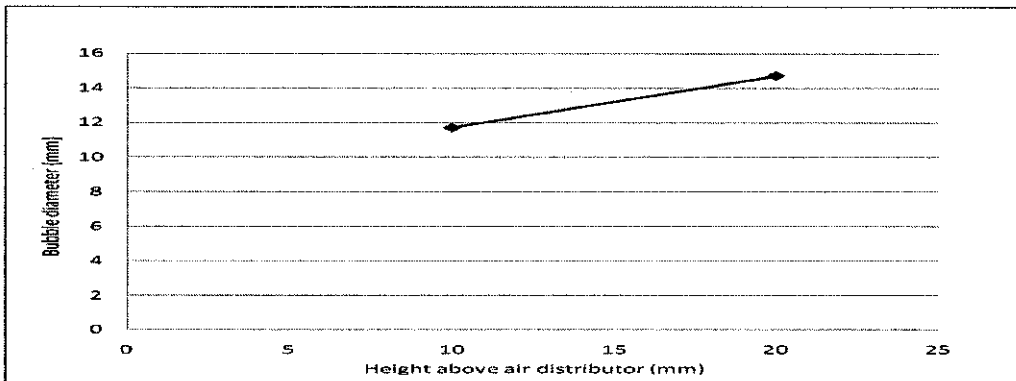


Figure 4.1: Bubble diameter versus height above air distributor for $D_p = 1.64\text{mm}$, $H_{mf} = 80\text{mm}$, Pressure = 0.25bar

At pressure of 0.25bar, as shown in Fig. 4.1, bubble diameter keep increasing for the range of height above air distributor are 10mm to 20mm. The formation of bubble diameter rupture afterward because it does not have enough pressure to push the sand upward. The 20mm height above air distributor is defined as the maximum bubble height, h^* for the condition of $D_p = 1.64\text{mm}$, $H_{mf} = 80\text{mm}$ and Pressure = 0.25bar

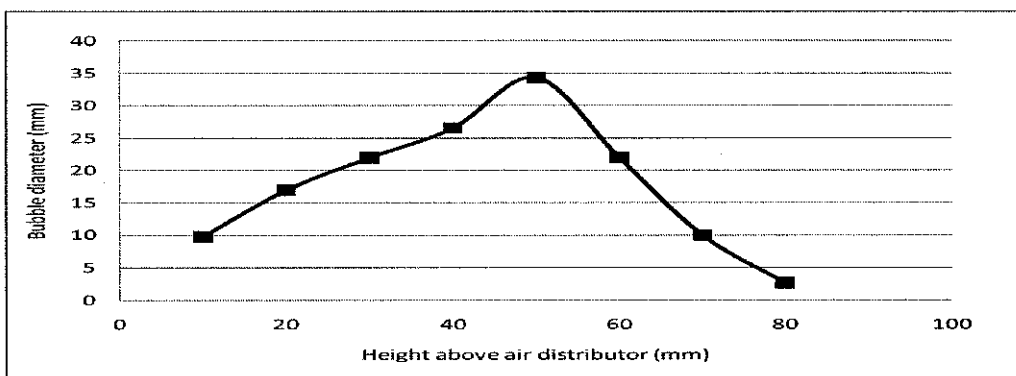


Figure 4.2: Bubble diameter versus height above air distributor for $D_p = 1.64\text{mm}$, $H_{mf} = 80\text{mm}$, Pressure = 0.5bar

At pressure of 0.5bar, as in Fig.4.2 bubble diameter keep increasing from height above air distributor are 10mm to 50mm. Beyond 50mm, the formation of bubble diameter is decreasing and split due to instabilities at the bubble boundary. The 50mm height above air distributor is defined as the maximum bubble height, h^* for the condition of $D_p = 1.64\text{mm}$, $H_{mf} = 80\text{mm}$ and Pressure = 0.5bar.

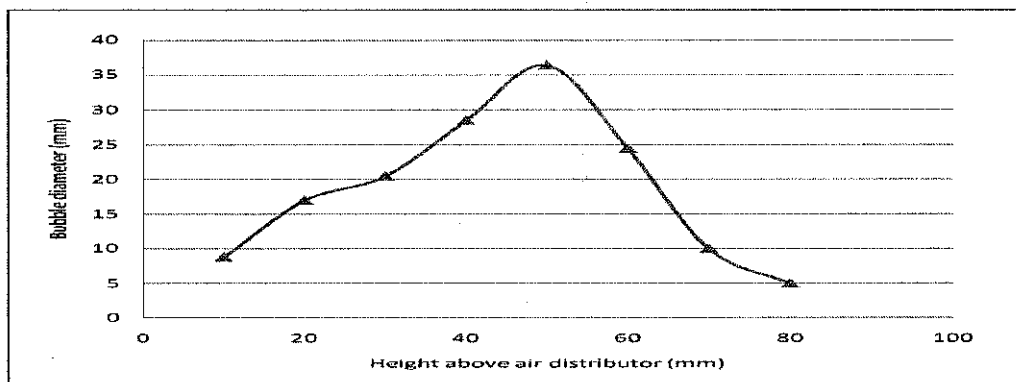


Figure 4.3: Bubble diameter versus height above air distributor for $D_p = 1.64\text{mm}$, $H_{mf} = 80\text{mm}$, Pressure = 0.75bar

At pressure of 0.75bar, as in Fig 4.3, bubble diameter keep increasing from height above air distributor is 10mm to 50mm. Beyond 50mm, the formation of bubble diameter are decreasing and split due to instabilities at the bubble boundary. The 50mm height above air distributor is defined as the maximum bubble height, h^* for the condition of $D_p = 1.64\text{mm}$, $H_{mf} = 80\text{mm}$ and Pressure = 0.75bar.

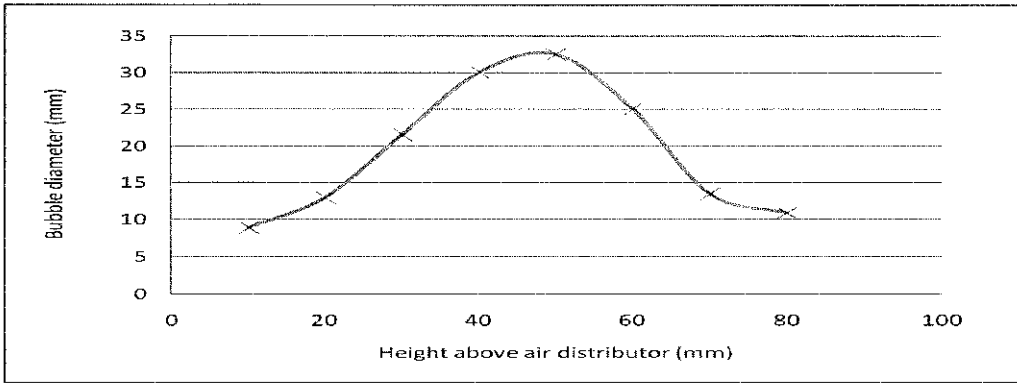


Figure 4.4: Bubble diameter versus height above air distributor for $D_p = 1.64\text{mm}$, $H_{mf} = 80\text{mm}$, Pressure = 1.0bar

At pressure of 1.0bar, as in Fig 4.4, bubble diameter keep increasing from height above air distributor are 10mm to 50mm. Beyond 50mm, the formation of bubble diameter is decreasing and split due to instabilities at the bubble boundary. The 50mm height above air distributor is defined as the maximum bubble height, h^* for the condition of $D_p = 1.64\text{mm}$, $H_{mf} = 80\text{mm}$ and Pressure = 1.0bar.

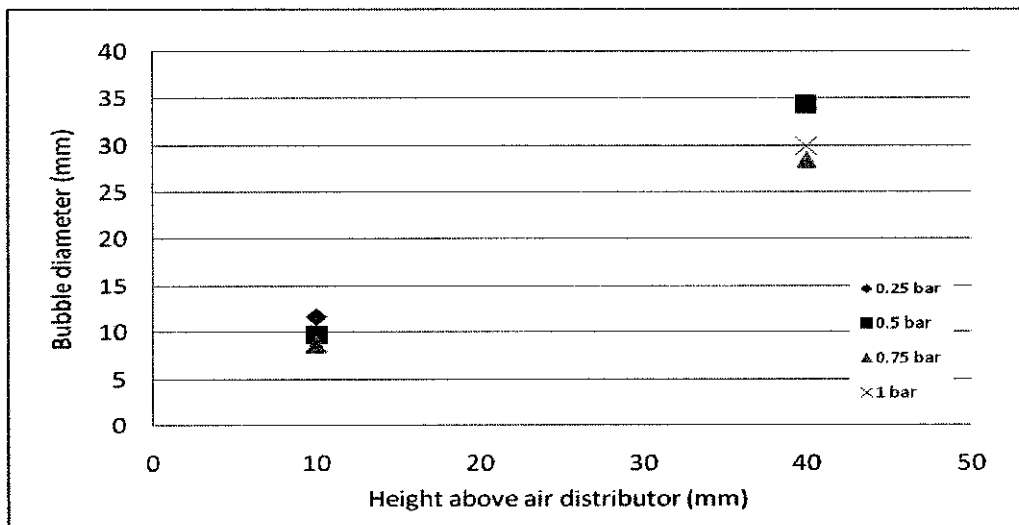


Figure 4.5: Bubble diameter versus height above air distributor, $D_p = 1.64\text{mm}$, $H_{mf} = 80\text{mm}$, Pressure = 0.25-1.0bar

Base on Fig. 4.5, at height above air distributor are 10mm and 40mm bubble diameter are decreasing with the increasing of pressure. At low pressure, bubble diameter easy to be form since it is small particle.

However, according to J.Wiman, 1998, at high pressure, an increased gas-particle interaction, in combination with turbulent fluctuation in the gas phase, can be used to explain the increased bubble instability with a corresponding increased bubble splitting. In this case, it explains why small bubble diameter will be form at high pressure.

The graph of bubble diameter at certain height above air distributor of 0.25, 0.5, 0.75 and 1.0 bar for $D_p = 2.36\text{mm}$ are shown in Fig. 4.6, Fig. 4.7, Fig. 4.8 and 4.9.

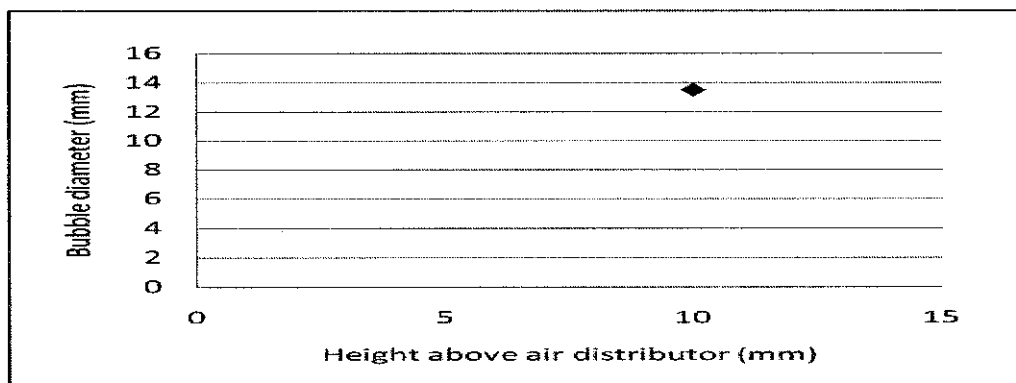


Figure 4.6: Bubble diameter versus height above air distributor for $D_p = 2.36\text{mm}$, $H_{mf} = 80\text{mm}$, Pressure = 0.25bar

At pressure of 0.25bar, as in Fig. 4.6, bubble form at height above air distributor is 10mm only. The formation of bubble diameter rupture afterward because it does not have enough pressure to push the sand upward. The 10mm height above air distributor is defined as the maximum bubble height, h^* for the condition of $D_p = 1.64\text{mm}$, $H_{mf} = 80\text{mm}$ and Pressure = 0.25bar.

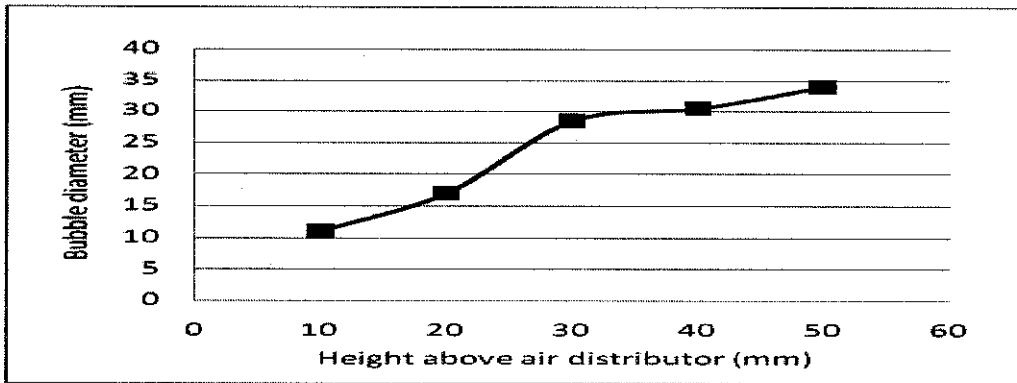


Figure 4.7: Bubble diameter versus height above air distributor for $D_p = 2.36\text{mm}$, $H_{mf} = 80\text{mm}$, Pressure = 0.5bar

At pressure of 0.5bar, as in Fig 4.7, bubble diameter keep increasing from height above air distributor are 10mm to 50mm. The formation of bubble diameter rupture afterward because it does not have enough pressure to push the sand upward. The 50mm height above air distributor is defined as the maximum bubble height, h^* for the condition of $D_p = 2.36\text{mm}$, $H_{mf} = 80\text{mm}$ and Pressure = 0.5bar.

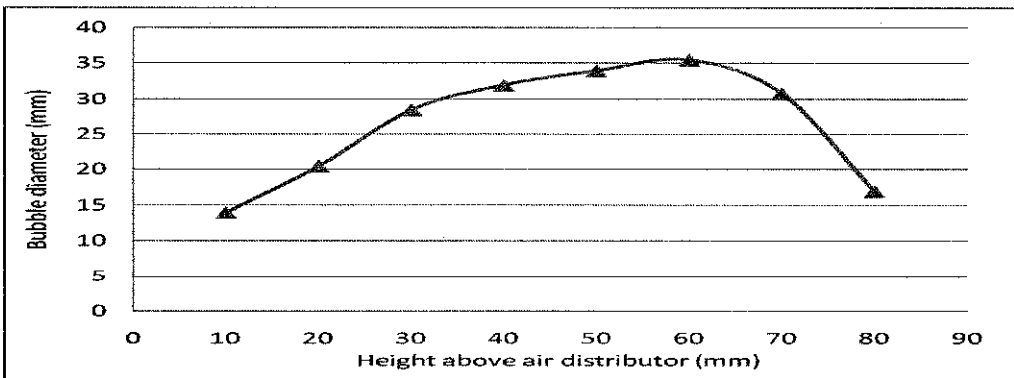


Figure 4.8: Bubble diameter versus height above air distributor for $D_p = 2.36\text{mm}$, $H_{mf} = 80\text{mm}$, Pressure = 0.75bar

At pressure of 0.75bar,as in Fig. 4.8, bubble diameter keep increasing from height above air distributor are 10mm to 60mm. Beyond 60mm, the formation of bubble diameter is decreasing and split due to instabilities at the bubble boundary. The 60mm height above air distributor is defined as the maximum bubble height, h^* for the condition of $D_p = 2.36\text{mm}$, $H_{mf} = 80\text{mm}$ and Pressure = 0.75bar.

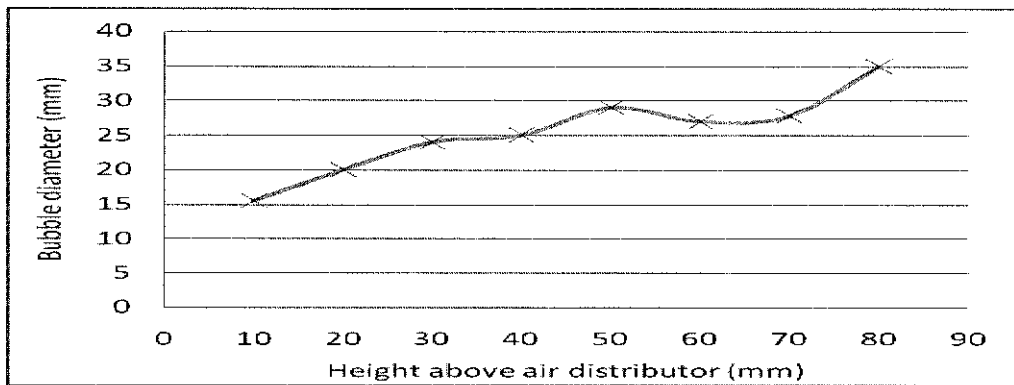


Figure 4.9: Bubble diameter versus height above air distributor for $D_p = 2.36\text{mm}$, $H_{mf} = 80\text{mm}$, Pressure = 1.0bar

At pressure of 1.0bar, as in Fig. 4.9, bubble diameter keep increasing from height above air distributor are 10mm to 50mm. Beyond 50mm, the formation of bubble diameter is decreasing and split due to instabilities at the bubble boundary. The 50mm height above air distributor is defined as the maximum bubble height, h^* for the condition of $D_p = 2.36\text{mm}$, $H_{mf} = 80\text{mm}$ and Pressure = 1.0bar.

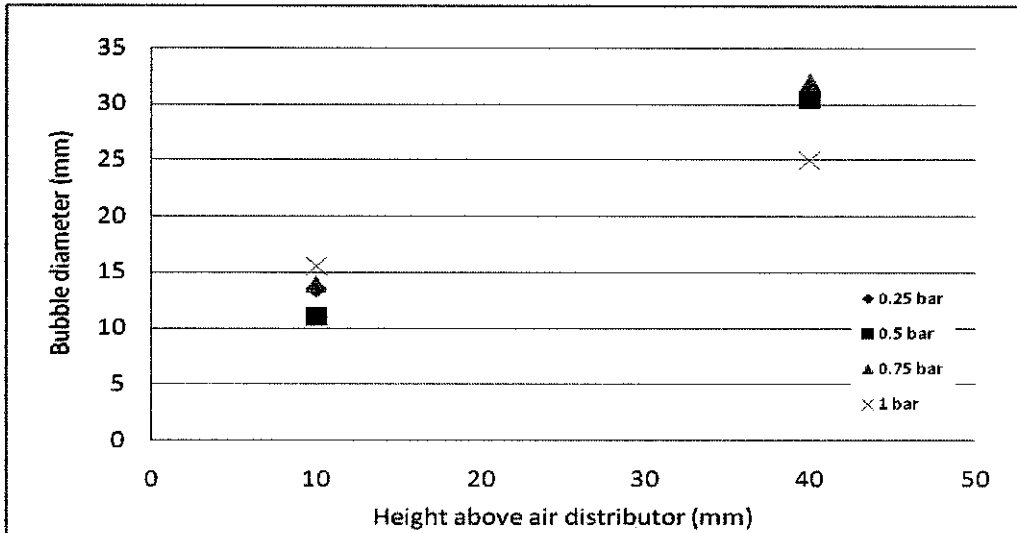


Figure 4.10: Bubble diameter versus height above air distributor for $D_p = 2.36\text{mm}$, $H_{mf} = 80\text{mm}$, Pressure = 0.25-1.0bar.

Base on Fig. 4.10, at height above air distributor is 10mm, bubble diameter is increasing with the increasing of pressure except at 0.25bar. The measurement at 0.25bar is happen because air pressure is centralized at the low height above air distributor region and created big bubble diameter. However, at height above air distributor is 40mm, bubble diameter is decreasing with the increasing of pressure. Compare to the bubble form in high pressure that rise in a bubbling fluidized bed and grow up rapidly in the beginning, the bubble in low pressure rise and grow up slowly and reach maximum value at high height above air distributor section.

The graph of bubble diameter at certain height above air distributor of 0.25, 0.5, 0.75 and 1.0 bar for $D_p = 3.35\text{mm}$ are shown in Fig. 4.11, Fig. 4.12, Fig. 4.13 and 4.14.

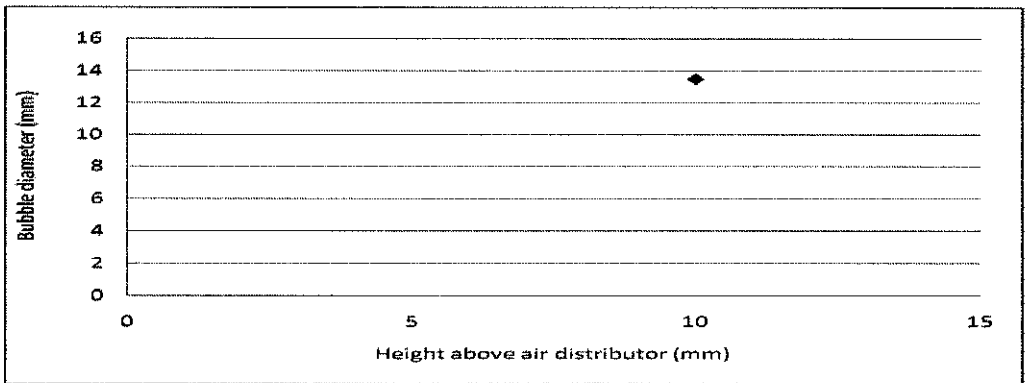


Figure 4.11: Bubble diameter versus height above air distributor for $D_p = 3.35\text{mm}$,
 $H_{mf} = 80\text{mm}$, Pressure = 0.25bar

At pressure of 0.25bar, as in Fig. 4.11, bubble form at height above air distributor is 10mm only. The formation of bubble diameter rupture afterward because it does not have enough pressure to push the sand upward. The 10mm height above air distributor is defined as the maximum bubble height, h^* for the condition of $D_p = 3.35\text{mm}$, $H_{mf} = 80\text{mm}$ and Pressure = 0.25bar

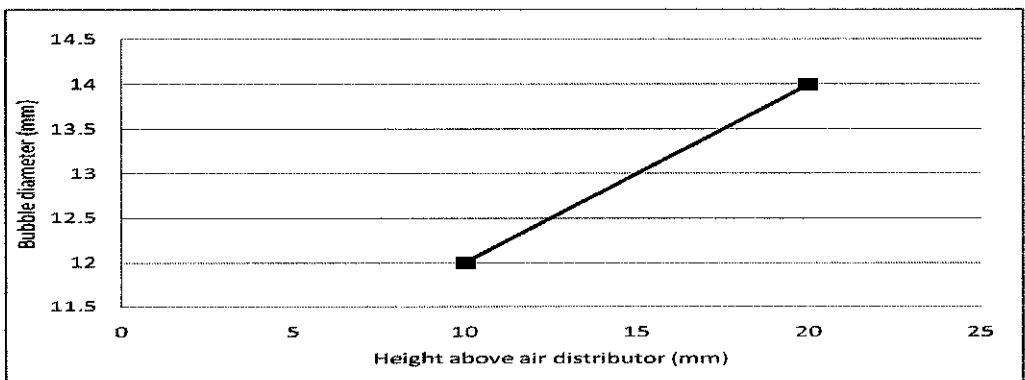


Figure 4.12: Bubble diameter versus height above air distributor for $D_p = 3.35\text{mm}$,
 $H_{mf} = 80\text{mm}$, Pressure = 0.5bar

At pressure of 0.5bar, as in Fig. 4.12, bubble diameter keep increasing from height above air distributor are 10mm to 20mm. The formation of bubble diameter rupture afterward because it does not have enough pressure to push the sand upward. The 20mm height above air distributor is defined as the maximum bubble height, h^* for the condition of $D_p = 3.35\text{mm}$, $H_{mf} = 80\text{mm}$ and Pressure = 0.25bar.

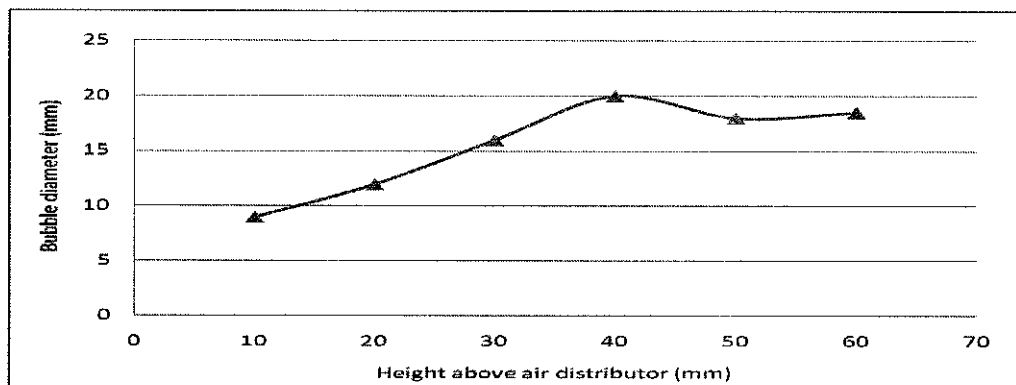


Figure 4.13: Bubble diameter versus height above air distributor for $D_p = 3.35\text{mm}$, $H_{mf} = 80\text{mm}$, Pressure = 0.75bar

At pressure of 0.75bar, as in Fig. 4.13, bubble diameter keep increasing from height above air distributor are 10mm to 40mm. Beyond 40mm, the formation of bubble diameter is decreasing and split due to instabilities at the bubble boundary. The 40mm height above air distributor is defined as the maximum bubble height, h^* for the condition of $D_p = 3.36\text{mm}$, $H_{mf} = 80\text{mm}$ and Pressure = 0.75bar.

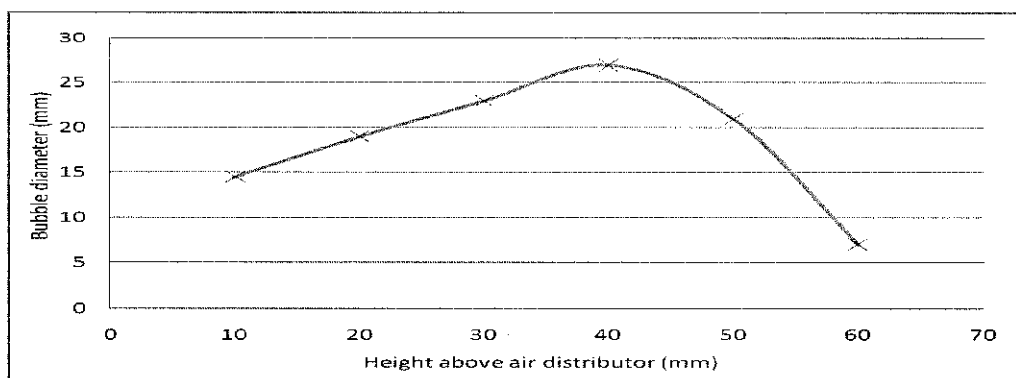


Figure 4.14: Bubble diameter versus height above air distributor for $D_p = 3.35\text{mm}$, $H_{mf} = 80\text{mm}$, Pressure = 1.0bar

At pressure of 1.0bar, as in Fig. 4.14, bubble diameter keep increasing from height above air distributor are 10mm to 40mm. Beyond 40mm, the formation of bubble diameter is decreasing and split due to instabilities at the bubble boundary. The 40mm height above air distributor is defined as the maximum bubble height, h^* for the condition of $D_p = 3.35\text{mm}$, $H_{mf}=80\text{mm}$ and Pressure= 1.0bar.

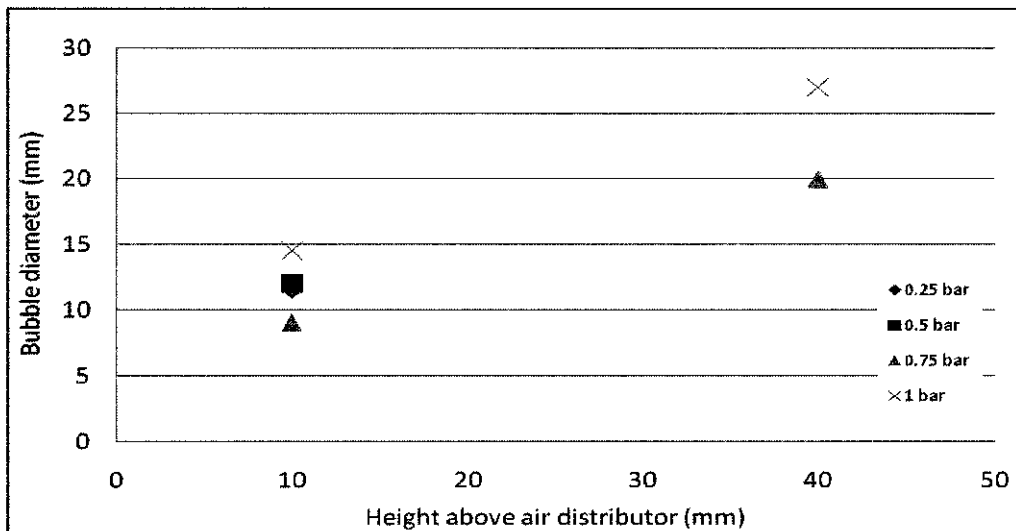


Figure 4.15: Bubble diameter versus height above air distributor for $D_p = 3.35\text{mm}$, $H_{mf} = 80\text{mm}$, Pressure = 0.25-1.0bar,

Base on Fig. 4.15, at height above air distributor is 10mm, bubble diameter is increasing with the increasing of pressure except at 0.25bar and 0.5bar. The measurement at 0.25bar is happen since it is the only data as in Fig 4.11 and the measurement at 0.5bar is been neglected since it form bubble up until 20mm height above air distributor only as in Fig 4.12. It mean the air pressure is centralized at the low height above air distributor region and created big bubble diameter although it been supply by a low pressure.

At height above air distributor is 40mm, bubble diameter is increasing with the increasing of pressure. Bubble diameter is keep increasing with pressure at both section, low and high height above air distribution is due to the size. Big particle, $D_p = 3.35\text{mm}$ is been used, that why high pressure is critical in order to produce high bubble diameter

4.1.2 Effect of particle diameter (D_p) to the bubble diameter at certain height above air distributor

The graph of bubble diameter at certain height above air distributor of $D_p = 1.64$, 2.36 and 3.35mm for 0.25, 0.5, 0.75 and 1.0 bar are shown in Fig. 4.16, Fig. 4.17, Fig. 4.18 and 4.19.

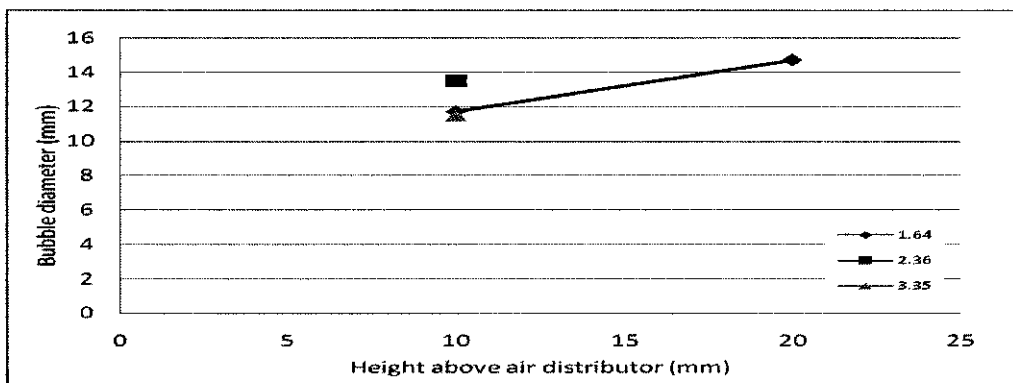


Figure 4.16: Bubble diameter versus height above air distributor for $D_p = 1.64$, 2.36 and 3.35mm, $H_{mf} = 50\text{mm}$, Pressure = 0.25bar

Base on Fig. 4.16, diameter particle, $D_p = 1.64$ form bubble up until 20mm height above air distributor compare than $D_p = 2.36$ and 3.35 that only form bubble up until 10mm height above air distributor only. This happen because $D_p = 1.64$ is small in term of size compare to $D_p = 2.36\text{mm}$ and $D_p = 3.35\text{mm}$. This characteristic makes bubble easy to be form and rise in a bubbling fluidized bed.

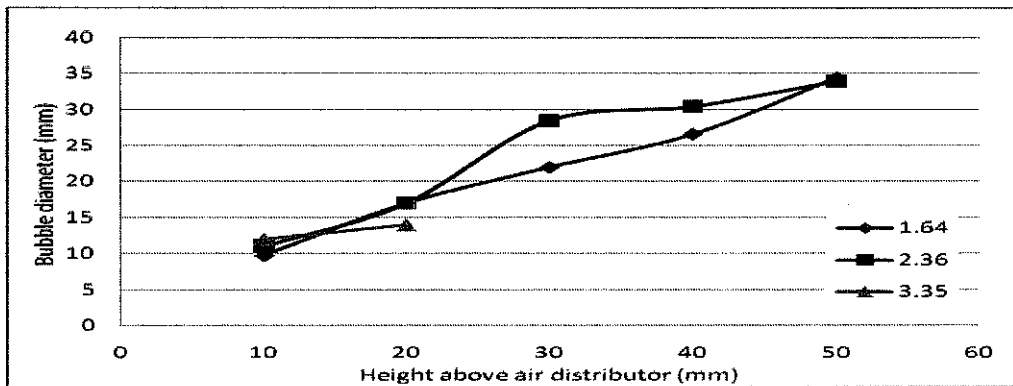


Figure 4.17: Bubble diameter versus height above air distributor for $D_p = 1.64, 2.36$ and 3.35mm , $H_{mf} = 50\text{mm}$, Pressure = 0.5bar

Base on Fig. 4.17, diameter particle, $D_p = 1.64$ and 2.36 form bubble up until 50mm height above air distributor compare than $D_p = 3.35$ that only form bubble up until 20mm height above air distributor only. This happen because $D_p = 3.35\text{mm}$ is big in term of size. This characteristic makes bubble difficult to be form and rise in a bubbling fluidized bed.

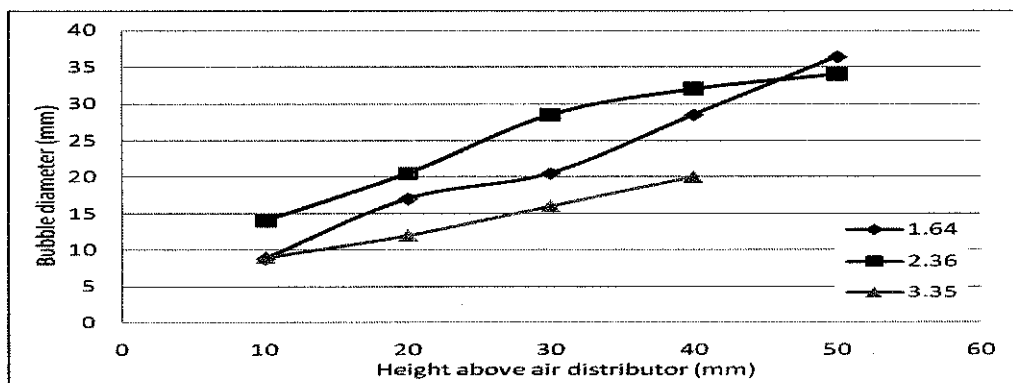


Figure 4.18: Bubble diameter versus height above air distributor for $D_p = 1.64, 2.36$ and 3.35mm , $H_{mf} = 50\text{mm}$, Pressure = 0.75bar

Base on Fig. 4.18, diameter particle, $D_p = 1.64$ and 2.36 form bubble up until 50mm height above air distributor compare than $D_p = 3.35$ that only form bubble up until 40mm height above air distributor only. This happen because $D_p = 3.35\text{mm}$ is big in term of size. This characteristic makes bubble difficult to be form and rise in a bubbling fluidized bed.

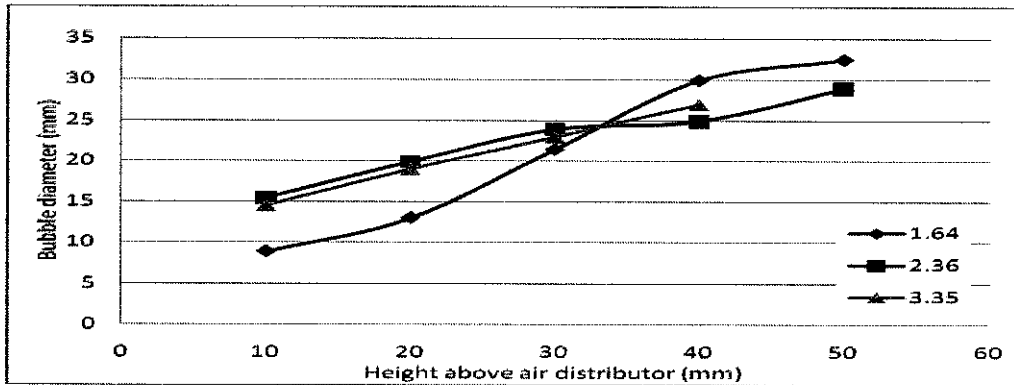


Figure 4.19: Bubble diameter versus height above air distributor for $D_p = 1.64, 2.36$ and 3.35 mm, $H_{mf} = 50$ mm, Pressure = 1.0 bar

Base on Fig. 4.19, diameter particle, $D_p = 1.64$ and 2.36 mm form bubble up until 50 mm height above air distributor compare than $D_p = 3.35$ mm that only form bubble up until 40 mm height above air distributor only. This happen because $D_p = 3.35$ mm is big in term of size. This characteristic makes bubble difficult to be form and rise in a bubbling fluidized bed.

4.2 BUBBLE DENSITY, δ_b

Experimental data about bubble density is calculated as in Appendix III. The results are show in Table 4.4, 4.5 and 4.6 for average particle diameters (D_p) of $1.64, 2.36$ and 3.35 mm and pressure of $0.25-1$ bar. Later, it been presented into Fig. 4. 20.

Table 4.4: Bubble density for $D_p = 1.64$ mm.

Pressure (bar)	Background	Particle	Bubble density
0.25	23.7315	10628.86	0.002228
0.5	95.1359	10349.86	0.009108
0.75	142.2488	7807.304	0.017894
1.0	249.1454	7708.108	0.03131

Table 4.5: Bubble density for $D_p = 2.36\text{mm}$.

Pressure (bar)	Background	Particle	Bubble density
0.25	18.9012	7258.19	0.002597
0.5	131.3981	7270.301	0.017752
0.75	64.684	7361.936	0.00871
1.0	198.4623	7253.08	0.026634

Table 4.6: Bubble density for $D_p = 3.35\text{mm}$.

Pressure (bar)	Background	Particle	Bubble density
0.25	49.073	7356.686	0.006626
0.5	140.9887	7276.111	0.019009
0.75	33.6721	7227.318	0.004637
1.0	160.73	7079.749	0.022199

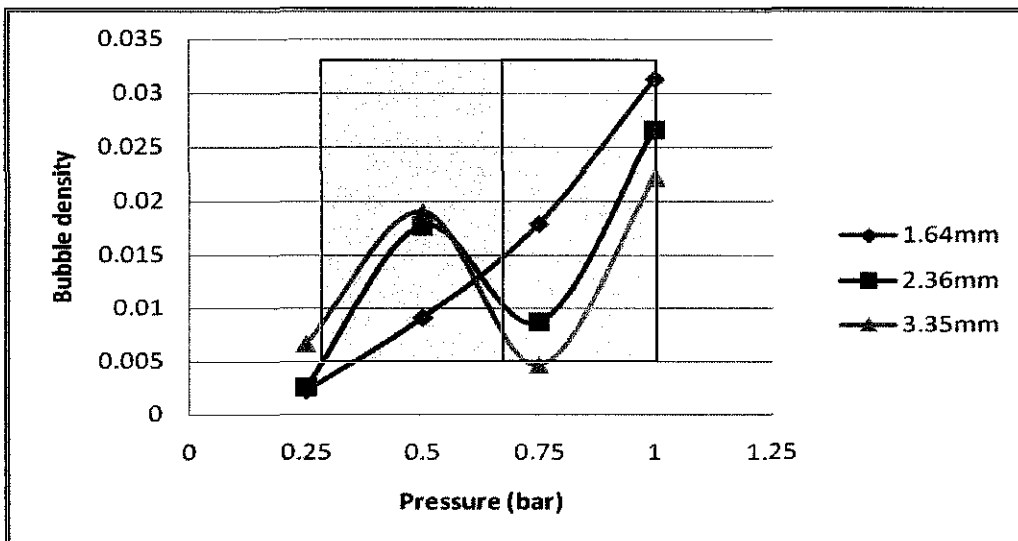


Figure 4.20: Bubble density versus pressure

Base on Fig. 4.20, it can be split into 2 regions; low and high pressure regions.. Bubble density is increase with particle size at low pressure (0.25 bar and 0.5 bar), first region. However, bubble density decrease with particle size at high pressure (0.75 bar and 1 bar), second region.

At low pressure, bubble density increases with the particle size. However, according J.Wiman, 1998, at high pressure, an increased gas-particle interaction, in combination with turbulent fluctuation in the gas phase, can be used to explain the increased bubble instability with a corresponding increased bubble splitting. In this case, it explains why small bubble diameter will be form at high pressure.

4.3 BED EXPANSIONS

Experimental data about bed expansion is calculated as in Appendix IV. The results are show in Table 4.7, 4.8 and 4.9 for average particle diameters (D_p) of 1.64mm, 2.36mm and 3.35mm and pressure of 0.25-1 bar. Later, it been presented into Fig. 4.21.

Table 4.7: Bed expansion for $D_p = 1.64\text{mm}$.

Pressure (bar)	Expended bed height (mm)
0.25	97.079
0.5	143.4
0.75	166
1.0	222.6163

Table 4.8: Bed expansion for $D_p = 2.36\text{mm}$.

Pressure (bar)	Expended bed height (mm)
0.25	90.5
0.5	95.043
0.75	102.579
1.0	109.8

Table 4.9: Bed expansion for $D_p = 3.35\text{mm}$.

Pressure (bar)	Expended bed height (mm)
0.25	92
0.5	93
0.75	94.6
1.0	105.679

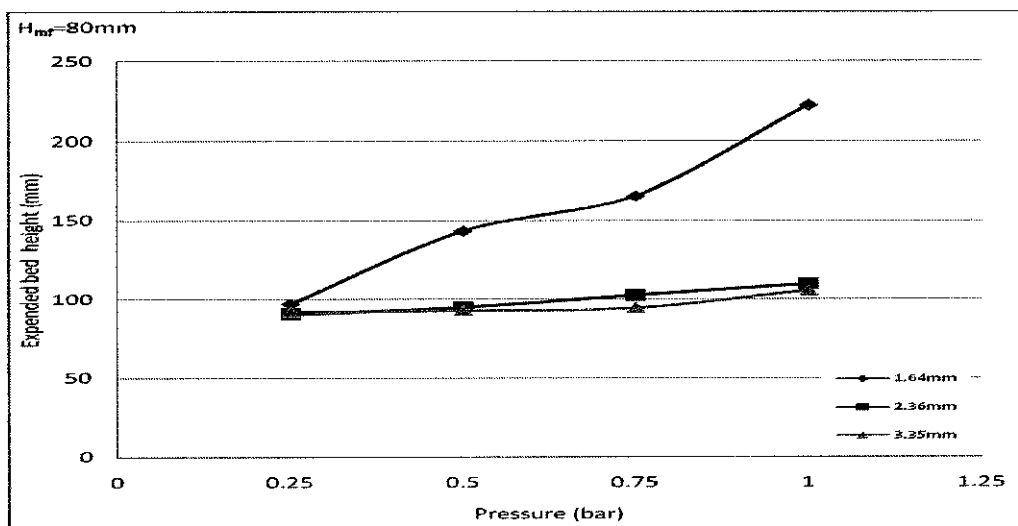


Figure 4.21: Expanded bed height versus Pressure

Base on Fig. 4.21, the results show that the bed new height consistently increases with increasing pressure. As shown in Fig. 4.21, there is a clear increase in the bubble activity with increasing pressure and generally also with excess gas velocity. At a similar pressure for the particle sizes investigated here (urea with the size of 2.36mm and 3.35mm), there is small significant influence of the particle size can be seen on the bed new height. The bed new height decreased with the particle size.

4.4: BUBBLE RISING VELOCITY, U_b

Experimental data about bubble rising velocity are calculated as in Fig. 3.8, 3.9 and the others in Appendix V. The results are show in Table 4.10, 4.11, 4.12 and 4.13 for average particle diameters (D_p) of 1.64mm with the pressure of 0.25-1 bar.

Table 4.10: Velocity for $D_p= 1.64\text{mm}$, 0.25bar

No	Height at Early point (cm)	Height at End point (cm)	The difference of height between Early point to End point (cm)	No. Picture for Early point	No. Picture for End point	The difference number of pictures	Time difference between Early point to End point (second)	Velocity (cm/s)	Average velocity (cm/s)
1 st	1.51	2.77	1.26	0024	0076	52	0.01733	72.7063	102.1154
2 nd	1.75	4.15	2.40					138.4615	
3 rd	1.60	3.25	1.65					95.1923	

Table 4.11: Velocity for $D_p= 1.64\text{mm}$, 0.5 bar

No	Height at Early point (cm)	Height at End point (cm)	The difference of height between Early point to End point (cm)	No. Picture for Early point	No. Picture for End point	The difference number of pictures	Time difference between Early point to End point (second)	Velocity (cm/s)	Average velocity (cm/s)
1 st	1.5	4.05	2.55	0100	0181	81	0.027	94.4444	105.5556
2 nd	4.2	7.35	3.15					116.6667	

Table 4.12: Velocity for $D_p= 1.64\text{mm}$, 0.75 bar

No	Height at Early point (cm)	Height at End point (cm)	The difference of height between Early point to End point (cm)	No. Picture for Early point	No. Picture for End point	The difference number of pictures	Time difference between Early point to End point (second)	Velocity (cm/s)	Average velocity (cm/s)
1 st	1.7	4.0	2.3	0097	0154	57	0.019	121.0526	160.5263
2 nd	1.8	5.6	3.8					200	

Table 4.13: Velocity for $D_p = 1.64\text{mm}$, 1.0 bar

No	Height at Early point (cm)	Height at End point (cm)	The difference of height between Early point to End point (cm)	No. Picture for Early point	No. Picture for End point	The difference number of pictures	Time difference between Early point to End point (second)	Velocity (cm/s)	Average velocity (cm/s)
1 st	3.76	5.5	1.74	0001	0031	30	0.01	174	167.5
2 nd	3.79	5.4	1.61					161	

Corresponding to Fig. 3.8, 3.9 and 49 to 54(Appendix V), the experimental data about the average bubble rising velocity, U_b , is shown in Table 4.10-4.13. By increasing the pressure from 0.25 to 1.0 bar, the bubble velocity is keep increase.

Ergun equation:

$$\Delta P = \frac{150 (1 - \varepsilon)^2 V \mu L}{\varepsilon^3 \Phi_s^2 D_p^2} + \frac{1.75 (1 - \varepsilon) \rho V^2 L}{\varepsilon^3 D_p \Phi_s} \quad (1)$$

where: ΔP is the pressure drop, ρ is density, kgm^{-3}

Φ_s is sphericity, V is superficial velocity, ms^{-1}

ε is void fraction, D_p is diameter particles, m

μ is viscosity, $\text{kgm}^{-1}\text{s}^{-1}$ L is depth of column, m

Evaluated from Ergun equation, the increasing of pressure drop may increase the superficial velocity. Thus, the result experiment of bubble rising velocity is supported by Ergun equation.

CHAPTER 5

CONCLUSIONS AND RECOMMENDATIONS

5.1 CONCLUSIONS

Films on the bubbling fluidized bed are captured using high speed camera. The high shutter speed feature is beneficial for capturing fast moving particle without a blurring effect, especially in the measurement of bubble movement. The application of digital image analysis can be done with the using of it. A qualitative and quantitative analysis of freely bubbling fluidized beds had been used to acquire data for understanding bubble diameter, bubble density, bed expansion and bubble rising velocity.

The results show that the bubble diameter increase with height above air distributor until maximum bubble height, h^* , beyond which bubbles do not grow further and become unstable and break up. The height h^* is a particle size dependency. As the density for all the particles are quite similar, it been considered as identical. By analyzing bubble diameter with the different pressure and size of particles, it can be seen that they are correlated; the graph look alike. The pattern of graph that is look alike, show minor effect of different pressure and size of particles toward bubble diameter.

The bubble density is not uniform throughout the bed cross section in the rectangular column. Bubble density increase with particle size at low pressure (0.25 bar and 0.5 bar), first region and decrease with particle size at high pressure (0.75 bar and 1 bar), second region.

The bed new height (bed expansion) is increase with pressure and decrease with particle size. Lastly, the result experiment of bubble rising velocity is supported by Ergun equation; increasing the pressure will increase the bubble velocity.

5.2 RECOMMENDATIONS

- i. By using more firm body of fluidized bed, a better result should be get since our study focusing on urea with is big size particles that need high pressure to fluidize.
- ii. The data from this experiment should be comparing with the experiment that has source of air moving like sprinkler system. Images of sand that source of air is unmoved as in Fig. 4.22(a) are compared with the images of sand that source of air moving like sprinkler system as Fig. 4.22 (b). It can be seen clearly that the sand is mixing more active. As a consequence, it may enhance fluidized bed reactors performance since that required an excellent mass and heat transfer.

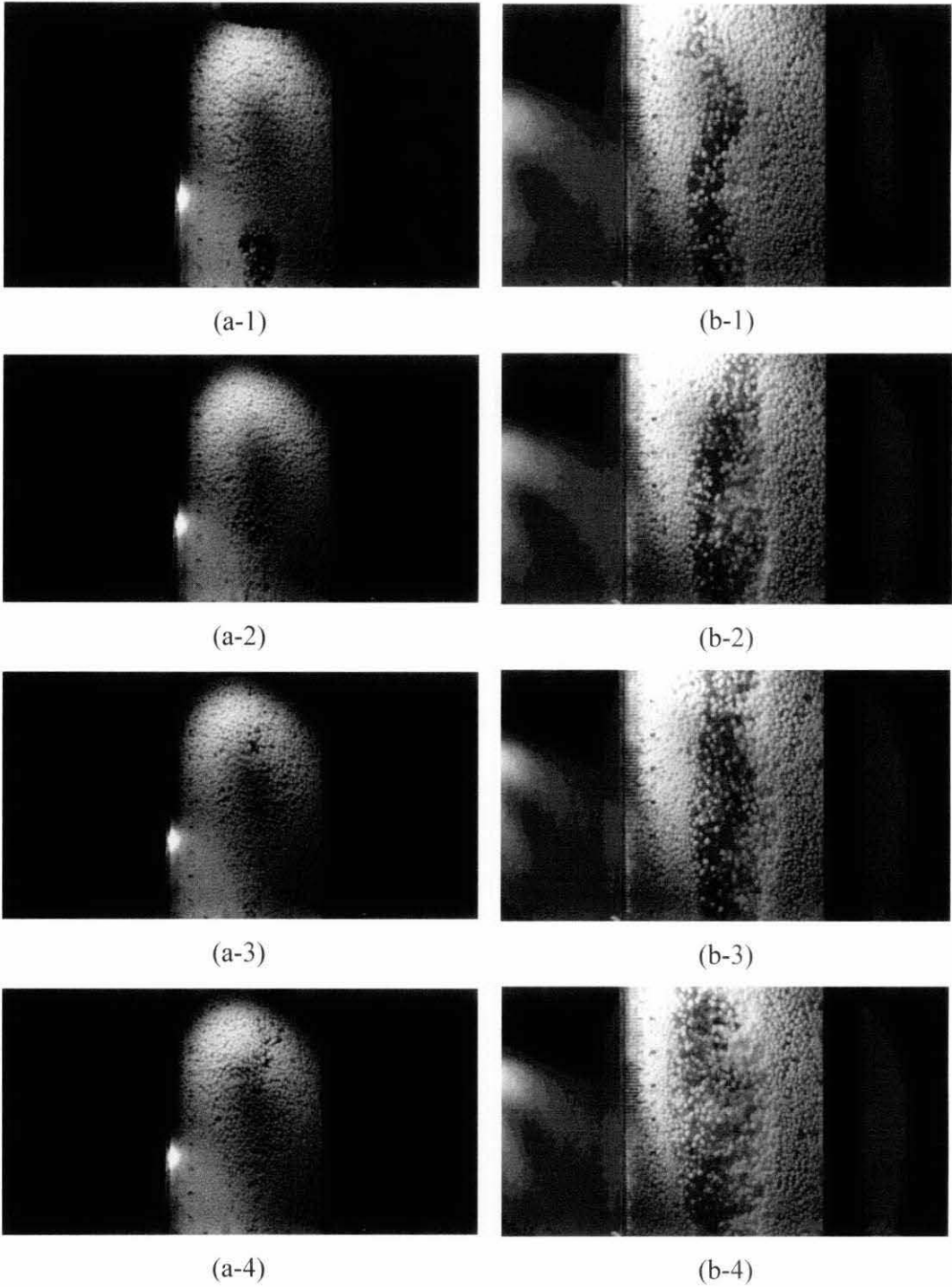


Figure 4.22: Image of sand with the $D_p = 1.64\text{mm}$, $H_{mf} = 80\text{mm}$, Pressure = 0.25 bar
 (a) source of air is unmoved (b) source of air moving like sprinkler system

REFERENCES

Bandyopadhyay, A. and Biswas, M.N., 2007. *Critical flow atomizer in SO₂ spray scrubbing*. Chemical Engineering Journal 139 (1): 29-41

Crites, T. and Turton, R., 2005. *Mathematical Model for the Prediction of Cycle-Time Distributions for the Wurster Column-Coating Process*. Ind. Eng. Chem. Res. 44 (14): 5397-5402

da Cunha, R.L.G., Pereira, M.M.C. and Rocha, S.C.S., 2009. *Conventional and modified fluidized bed: Comparison of the fluid dynamics and application in particle granulation*. Chemical Engineering and Processing: Process Intensification 48 (5): 1004-1011

Gauthier, D., Zerguerras, S. and Flamant, G., 1999. *Influence of the particle size distribution of powders on the velocities of minimum and complete fluidization*. Chemical Engineering Journal 74: 181-196

Geldart, D., 1973. *Types of gas fluidization*. Powder Technology 7 (5): 285-292

Heckötter, U., Larsson, A., Sriamornsak, P., and Vollrath, M.K., 2011. *Effect of annealing time and addition of lactose on release of a model substance from Eudragit RS coated pellets produced by a fluidized bed coater*. Chemical Engineering Research and Design 89 (6):697-705

Heinrich, S., Henneberg, M., Peglow, M., Drechsler, J. and Morl, L., 2005. *Fluidized bed spray granulation: analysis of heat and mass transfers and dynamic particle populations*. Braz. J. Chem. Eng 22 (2): 181-194

KuShaari, K.Z., 2003. *Modelling of Product Variability in Fluidized Bed Coating Equipment*. MSc Thesis. West Virginia University.

Leung, L.S., 1972. *Design of gas distributors and prediction of bubble size in large gas–solids fluidized beds*. Powder Technol **6 (4)**: 189–193

Pandey, S.K., 2010. *CFD Simulation of Hydrodynamics of Three Phase Fluidized Bed*. MSc Thesis. National Institute of Technology, India

Rajniak, P., Mancinelli, C., Chern, R.T., Stepanek, F., Farber, L. and Hill, B.T., 2007. *Experimental study of wet granulation in fluidized bed: Impact of the binder properties on the granule morphology*. International Journal of Pharmaceutics **334 (1-2)**: 92-102

Rajniak P., Stepanek F., Dhanasekharan K., Fan R., Mancinelli C. and Chern R., 2009. *A combined experimental and computational study of wet granulation in a Wurster fluid bed granulator*. Powder Technology **189 (2)**: 190-201

Roghair, I., 2007. *Development of an Experimental Method to Investigate the Hydrodynamics in a Fluidized Bed using PIV and DIA*. University of Twente

Shen, L., Johnsson, L. and Leckner, B., 2004. *Digital image analysis of hydrodynamics two-dimensional bubbling fluidized beds*. Chemical Engineering Science **59 (13)**: 2607-2617

Subramanian, G., Turton, R., Shelukar, S. and Flemme, L., 2003. *Effect of Tablet Deflectors in the Draft Tube of Fluidized/Spouted Bed Coaters* Ind. Eng. Chem. Res **42 (12)**: 2470–2478

Turton, R., 2008. *Challenges in the modeling and prediction of coating of pharmaceutical dosage forms*. Powder Technology **181 (2)**: 186–194

Vashishtha, M., Dongara, P. and Singh, D., 2010. *Improvement in Properties of Urea by Phosphogypsum Coating*. International Journal of ChemTech Research **2 (1)**: 36-44

Walker, G.M., Bell, S.E.J., Greene, K., Jones, D.S. and Andrews, G.P., 2009. *Characterisation of fluidised bed granulation processes using in-situ Raman spectroscopy*. Chemical Engineering Science **64 (1)**: 91–98

Zhou, T. and Li, H., 1999. *Effects of adding different size particles on fluidization of cohesive particles*. Powder Technology **102 (3)**: 215–220

APPENDICES

Appendix I

Example calculation of velocity:

(1st):

i. The difference of height between Early point to End point (cm)

Height at End point (cm)- Height at Early point (cm)

$$2.77-1.51= 1.26$$

ii. The difference number of pictures

No. picture for End point - No. picture for Early point

$$76-24 = 52$$

iii. Time difference from Early point to End point

The camera will take 3 000 pictures per second

$$3\ 000\ \text{pictures} = 1\ \text{second}$$

Thus, to take 52 pictures, the time needed is

$$\frac{1\ \text{second}}{3000\ \text{pictures}} \times 52\ \text{pictures} = 0.01733\ \text{second}$$

iv. Velocity

$$\frac{\text{The difference of height between Early point to End point (cm)}}{\text{Time difference between Early point to End point (second)}}$$

$$\frac{1.26\text{cm}}{0.01733\ \text{second}}$$

$$=72.7063\text{cm/s}$$

v) Average velocity

$$\frac{1^{\text{st}} \text{ velocity} + 2^{\text{nd}} \text{ velocity} + 3^{\text{rd}} \text{ velocity}}{3}$$

$$= \frac{(72.7063 + 138.4615 + 95.1923)}{3}$$

$$= 102.1154 \text{ cm/s}$$

Appendix II

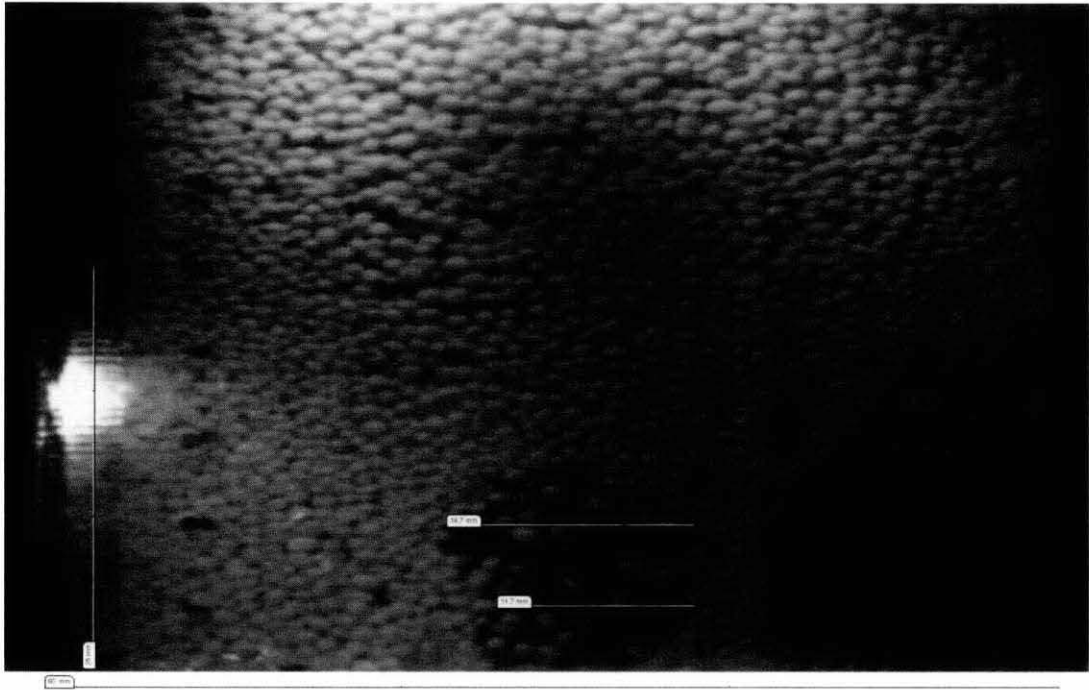


Figure 1: Bubble diameter distributions for height above air distributor. $D_p= 1.64\text{mm}$,
Pressure= 0.25 bar

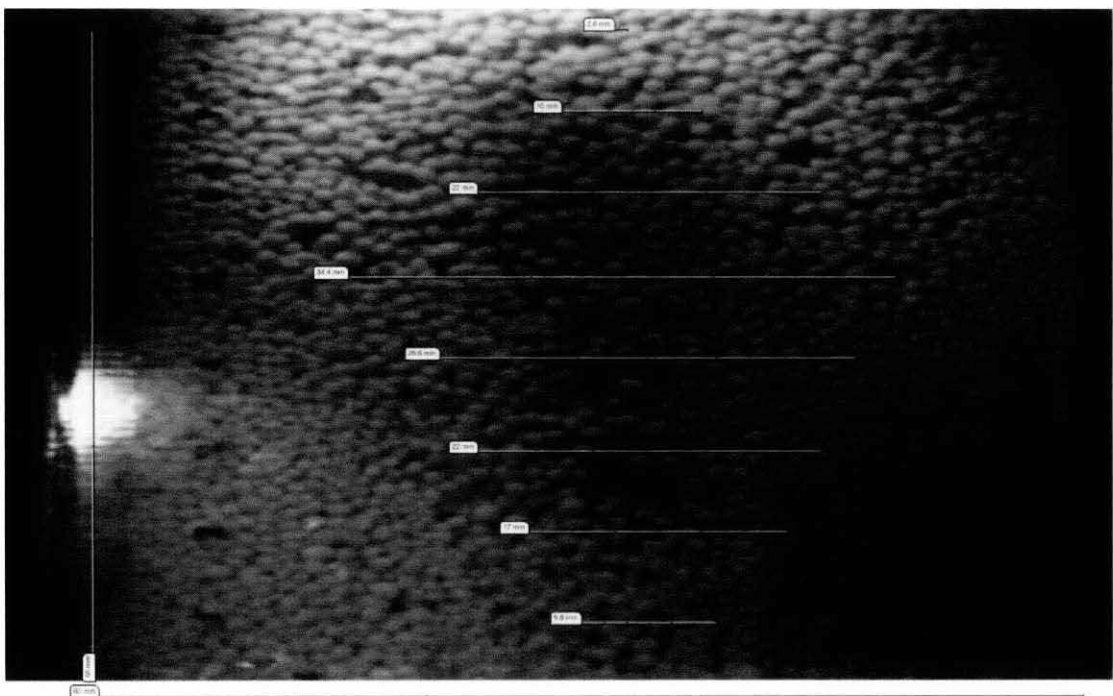


Figure 2: Bubble diameter distributions for height above air distributor. $D_p= 1.64\text{mm}$,
Pressure= 0.5 bar

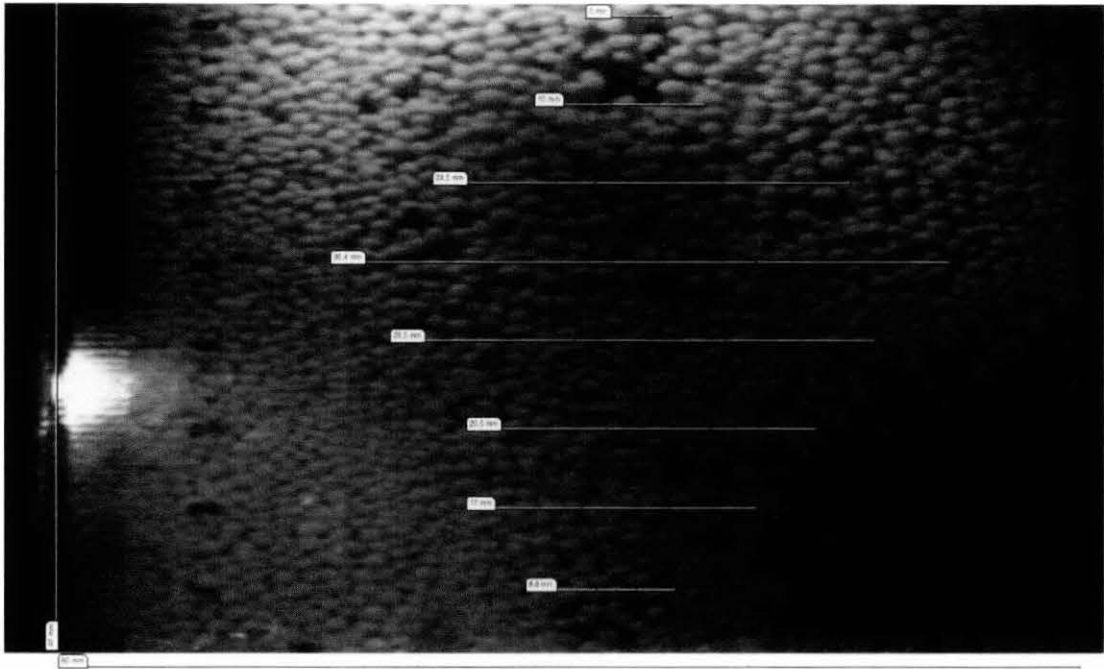


Figure 3: Bubble diameter distributions for height above air distributor. $D_p= 1.64\text{mm}$,
 Pressure= 0.75 bar

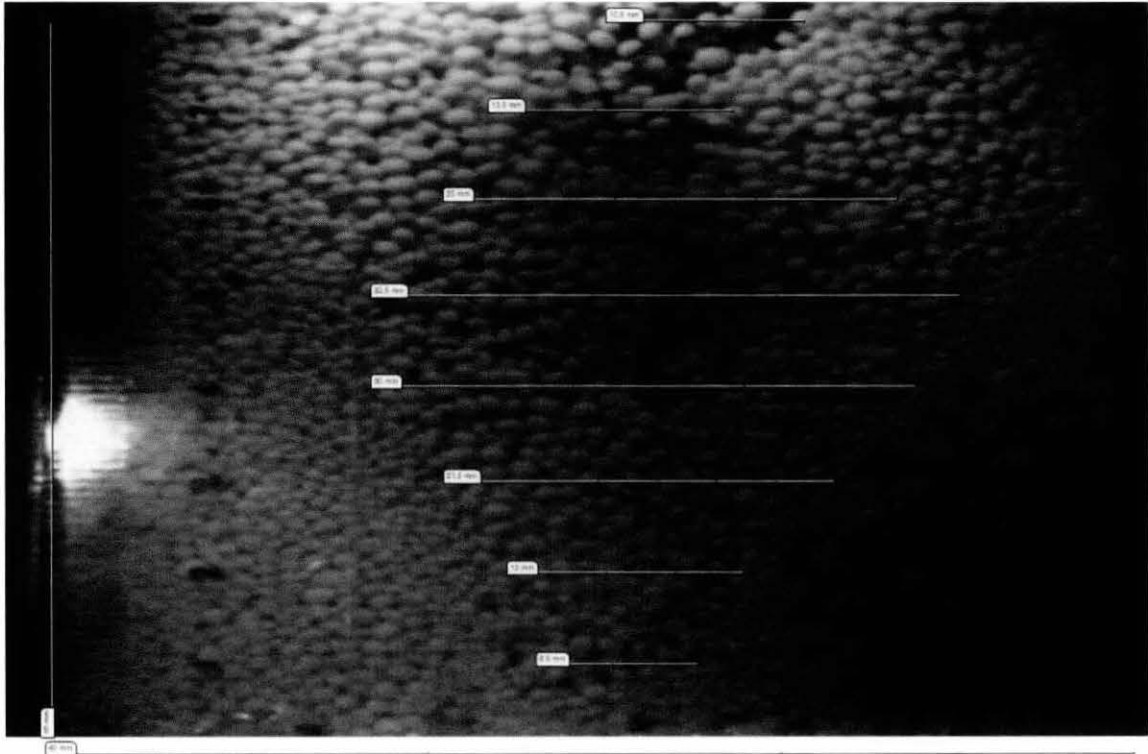


Figure 4: Bubble diameter distributions for height above air distributor. $D_p= 1.64\text{mm}$,
 Pressure= 1.0 bar

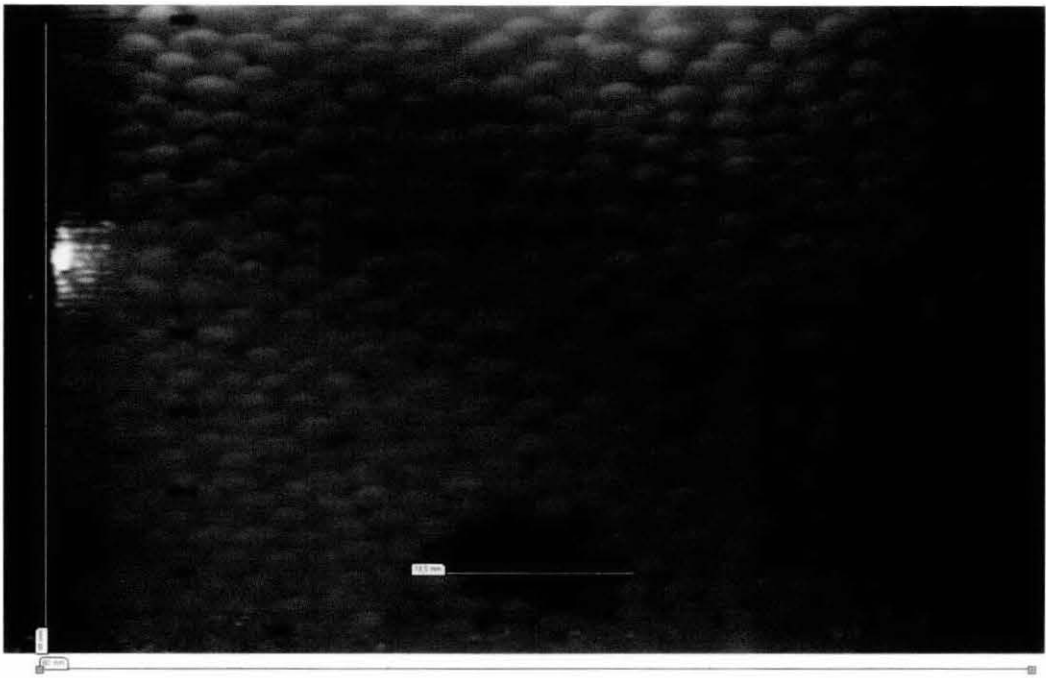


Figure 5: Bubble diameter distributions for height above air distributor. $D_p= 2.36\text{mm}$,
Pressure= 0.25 bar

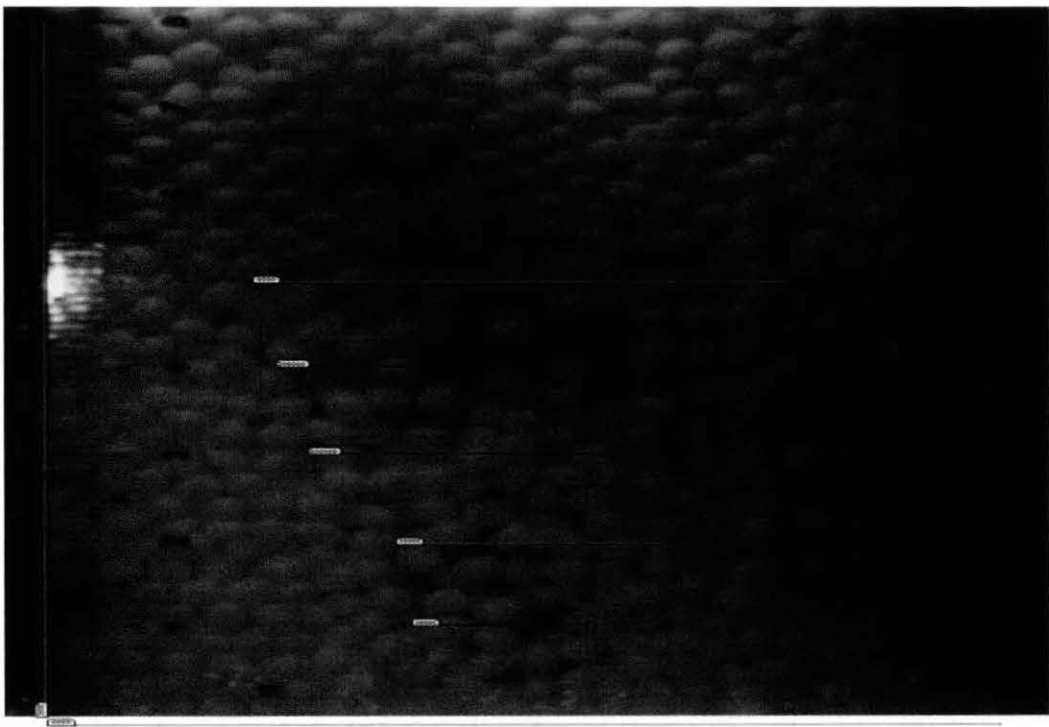


Figure 6: Bubble diameter distributions for height above air distributor. $D_p= 2.36\text{mm}$,
Pressure= 0.5 bar

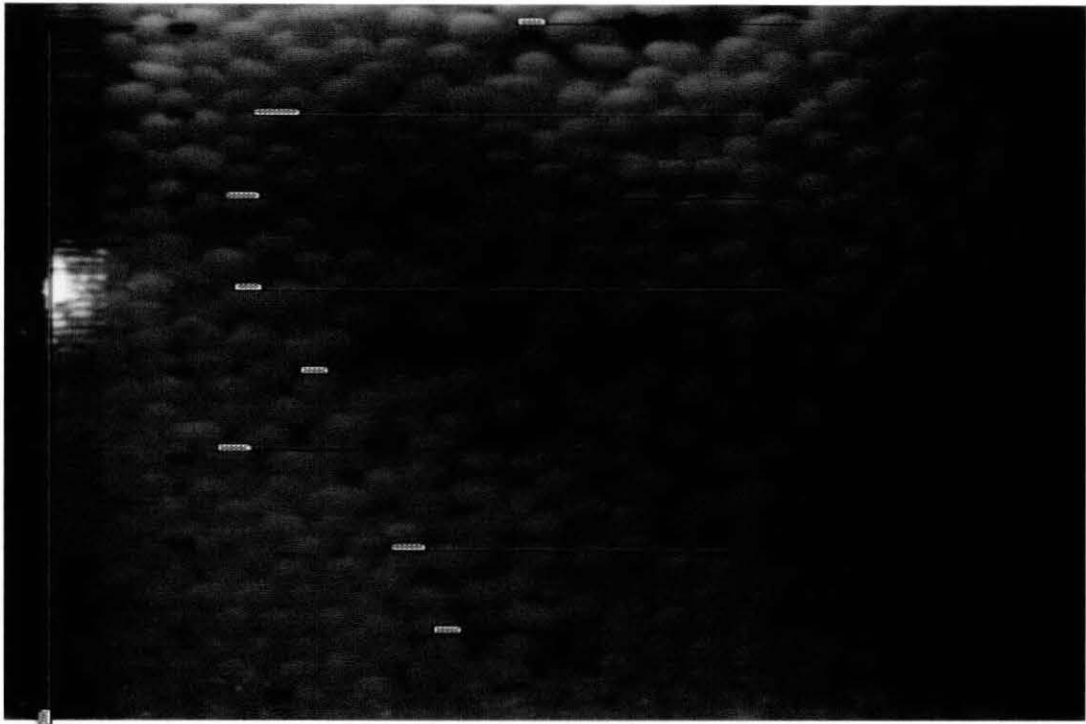


Figure 7: Bubble diameter distributions for height above air distributor. $D_p = 2.36\text{mm}$,
Pressure = 0.75 bar

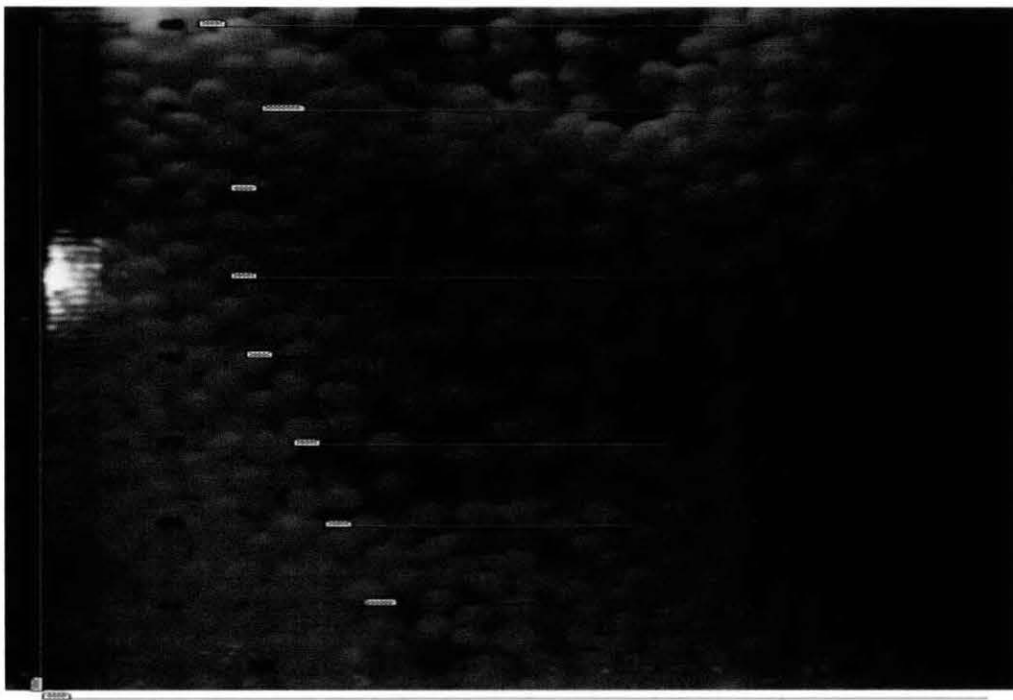


Figure 8: Bubble diameter distributions for height above air distributor. $D_p = 2.36\text{mm}$,
Pressure = 1.0 bar

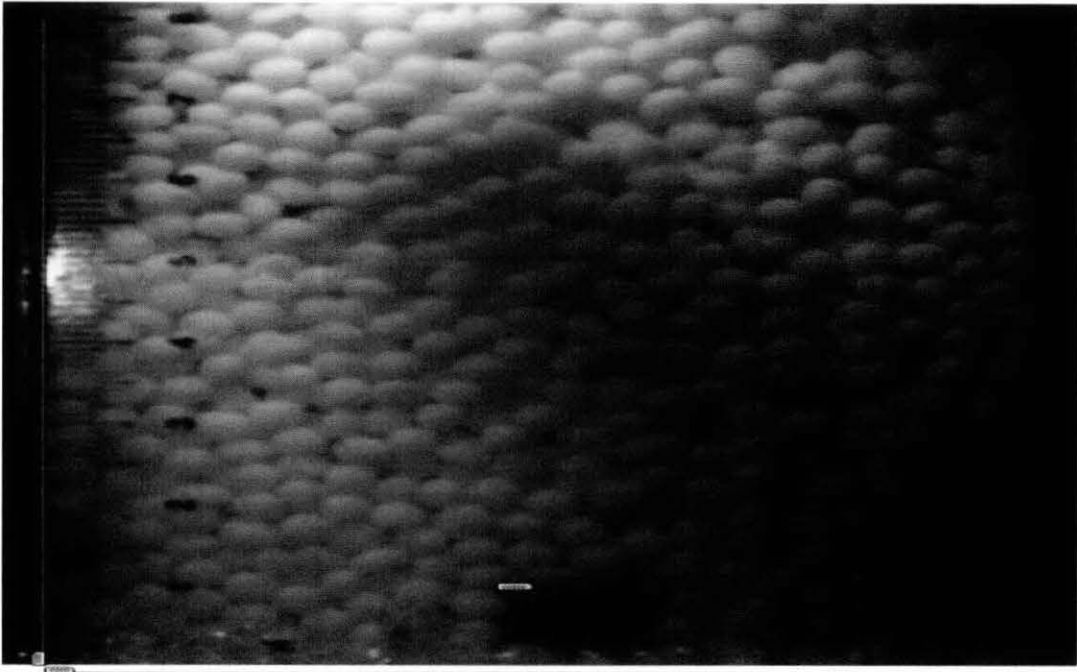


Figure 9: Bubble diameter distributions for height above air distributor. $D_p = 3.35\text{mm}$,
Pressure = 0.25 bar

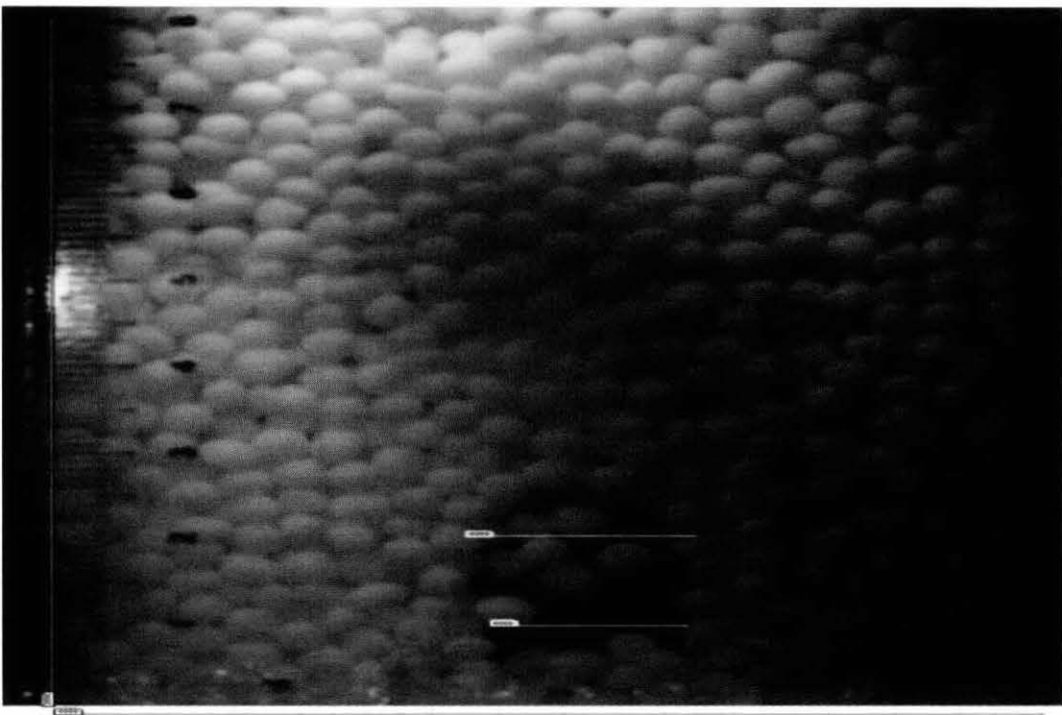


Figure 10: Bubble diameter distributions for height above air distributor. $D_p = 3.35\text{mm}$, Pressure = 0.5 bar

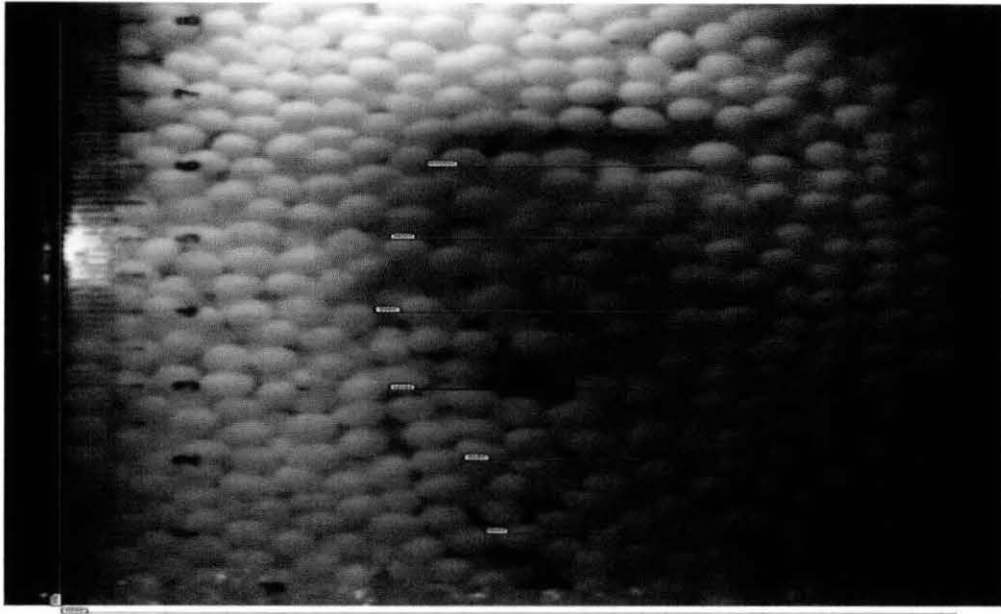


Figure 11: Bubble diameter distributions for height above air distributor.

$D_p=3.35\text{mm}$, Pressure= 0.5 bar

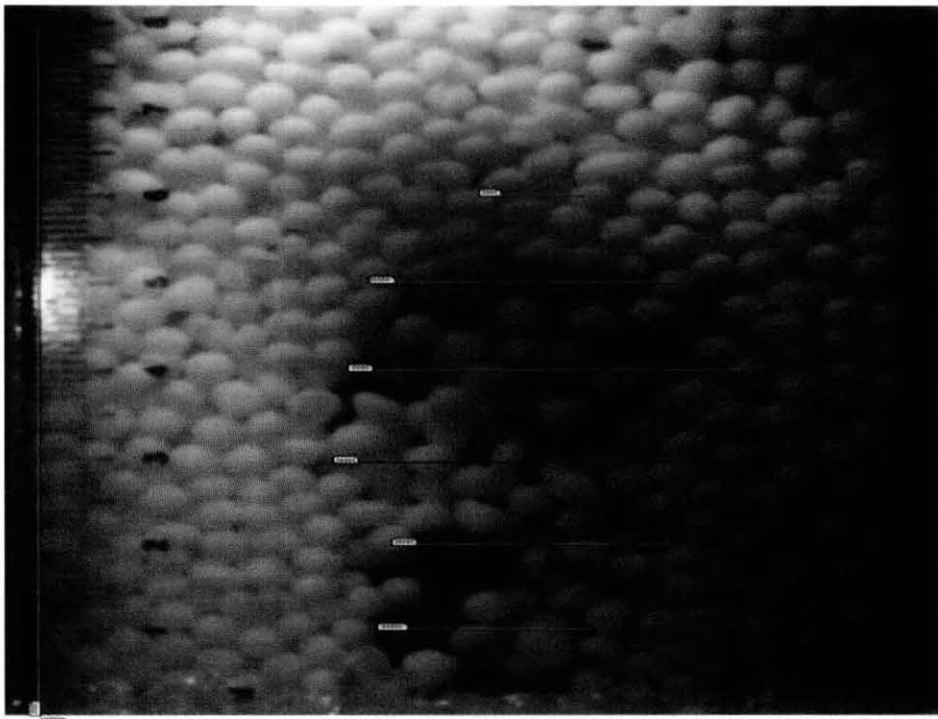


Figure 12: Bubble diameter distributions for height above air distributor. $D_p=$

3.35mm, Pressure= 1.0 bar

Appendix III

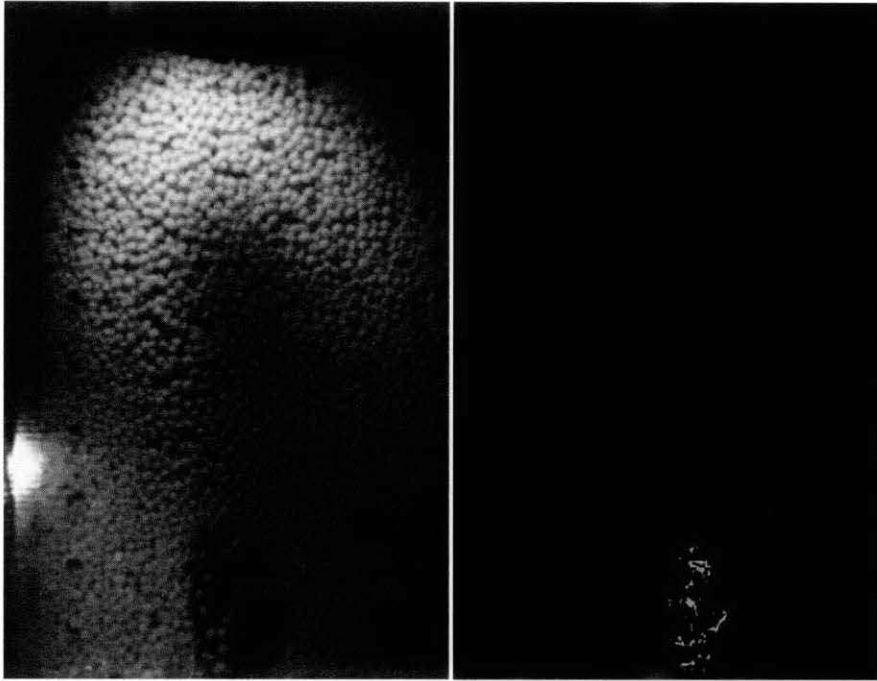


Figure 13: Principle of digital image analysis for a bubble density (a) original image (b) binary image for $D_p = 1.64\text{mm}$, 0.25 bar

All surface area distances are in square mm	
Whole image	
Yellow area	Picture total area: 10651.8601
0	Area black: 10628.1286
Black area	Area yellow: 0
10628.1286	Background (Gray): 23.7315
Yellow + Black area	Area A:
10628.1286	Area B:
Background (Gray)	Area A+B: 0
23.7315	Relation black to yellow+black: 100%
	Relation yellow to yellow+black: 0%
Memory Area B	
<input type="button" value="M+"/> <input type="button" value="M-"/>	<input type="button" value="R"/>
Memory Area A	
<input type="button" value="M+"/> <input type="button" value="M-"/>	<input type="button" value="R"/>

Figure 14: Calculation of bubble density for $D_p = 1.64\text{mm}$, 0.25 bar

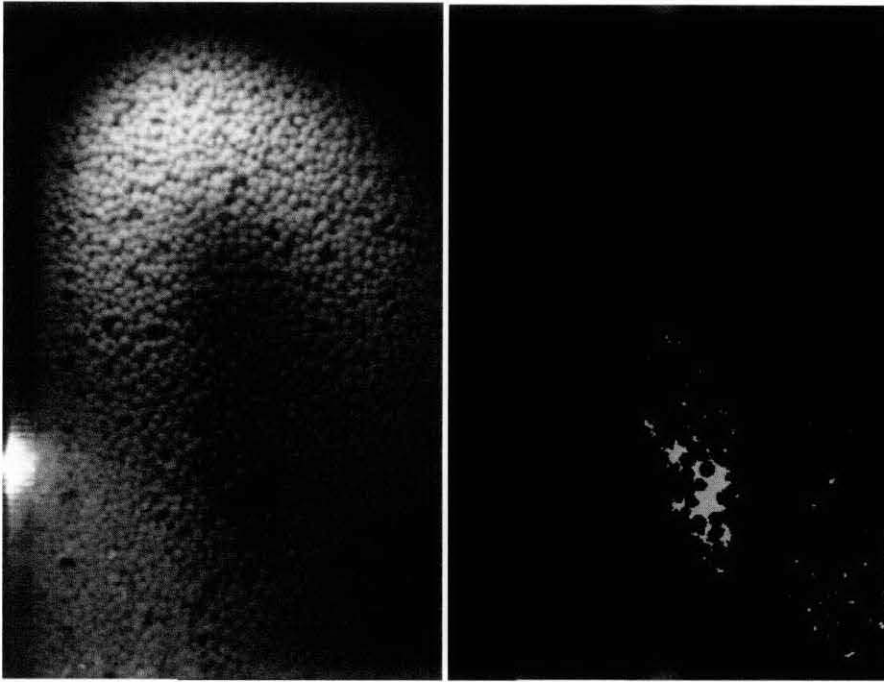


Figure 15: Principle of digital image analysis for a bubble density (a) original image (b) binary image for $D_p = 1.64\text{mm}$, 0.5 bar

All surface area distances are in square mm

Whole image	
Yellow area 5.2503	Picture total area: 10450.2476
Black area 10349.8614	Area black: 10349.8614
Yellow + Black area 10355.1117	Area yellow: 5.2503
Background (Gray) 95.1359	Background (Gray): 95.1359
	Area A:
	Area B:
	Area A+B: 0
	Relation black to yellow+black: 99.98%
	Relation yellow to yellow+black: 0.05%
Memory Area B	
M+ M-	R
Memory Area A	
M+ M-	R

Figure 16: Calculation of bubble density for $D_p = 1.64\text{mm}$, 0.5 bar

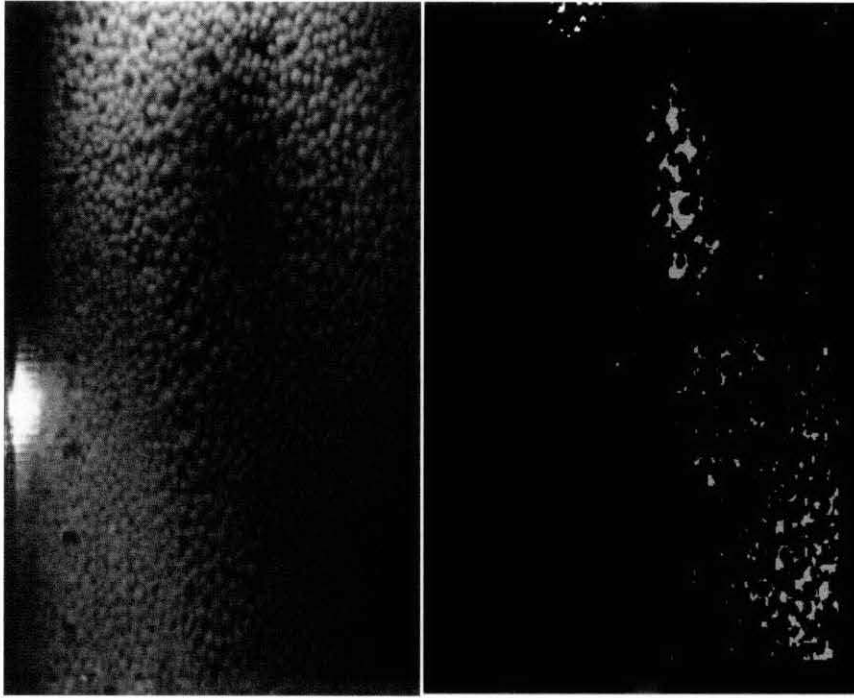


Figure 17: Principle of digital image analysis for a bubble density (a) original image (b) binary image for $D_p= 1.64\text{mm}, 0.75 \text{ bar}$

All surface area distances are in square mm

Whole image	
Yellow area	4.2703
Black area	7807.3038
Yellow + Black area	7811.5741
Background (Gray)	142.2488

Picture total area:	7953.8229
Area black:	7807.3038
Area yellow:	4.2703
Background (Gray):	142.2488

Area A:	
Area B:	
Area A+B:	0

Relation black to yellow+black:	99.96%
Relation yellow to yellow+black:	0.05%

Memory Area B

M+ M- R

Memory Area A

M+ M- R

Figure 18: Calculation of bubble density for $D_p= 1.64\text{mm}, 0.75 \text{ bar}$

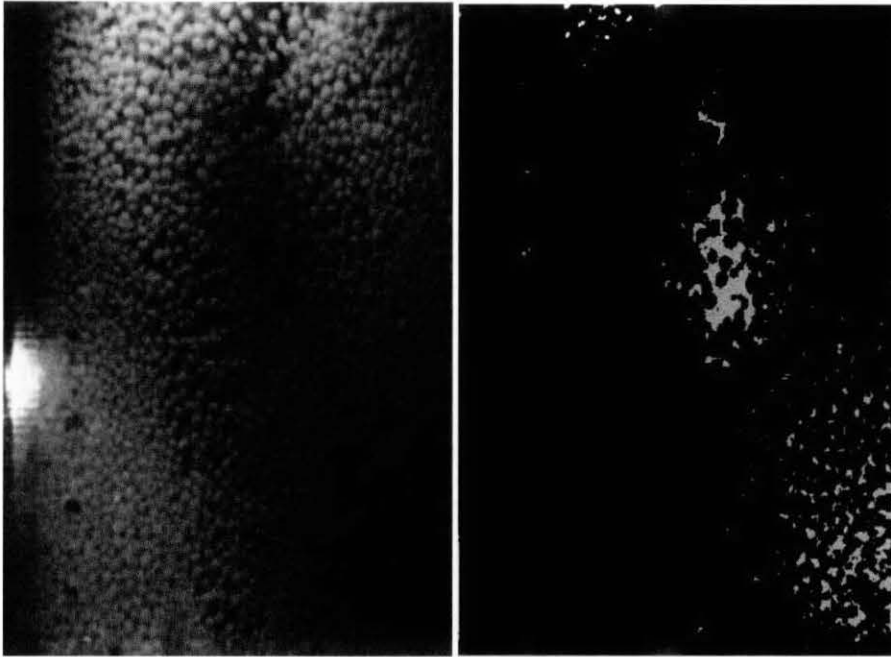


Figure 19: Principle of digital image analysis for a bubble density (a) original image (b) binary image for $D_p = 1.64\text{mm}$, 1.0 bar

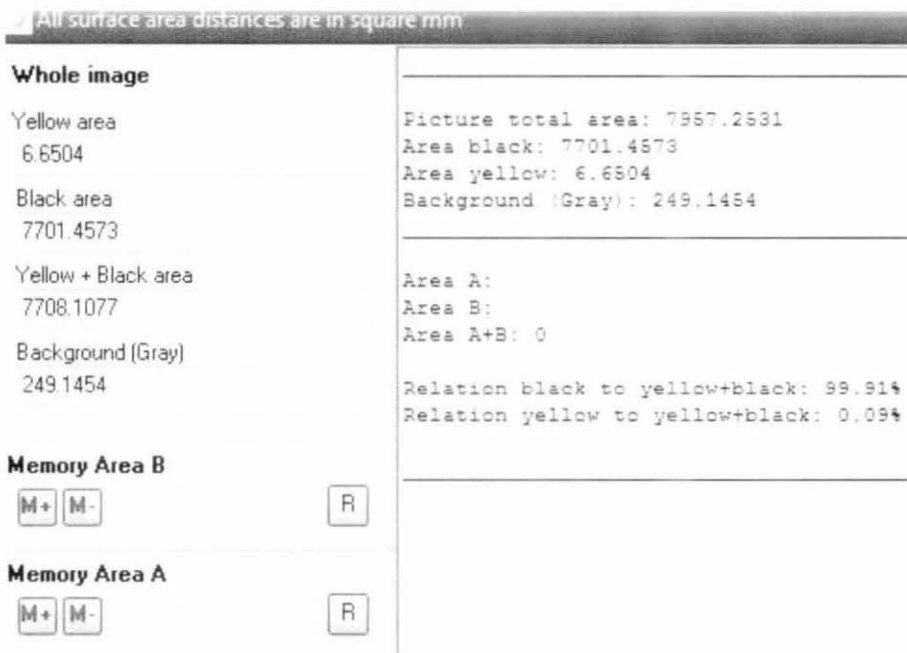


Figure 20: Calculation of bubble density for $D_p = 1.64\text{mm}$, 1.0 bar

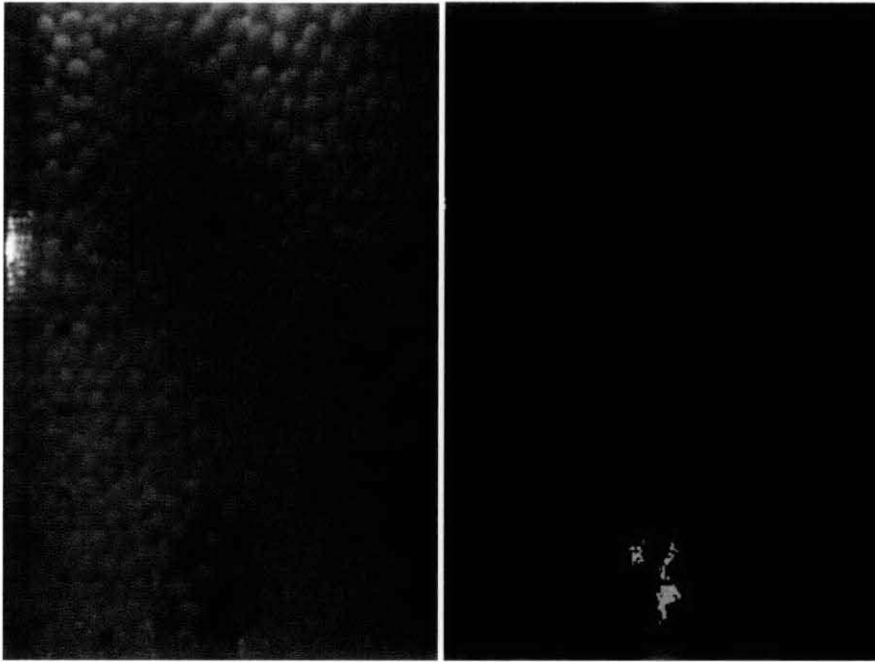


Figure 21: Principle of digital image analysis for a bubble density (a) original image (b) binary image for $D_p= 2.36\text{mm}$, 0.25 bar

All surface area distances are in square mm

Whole image	
Yellow area	Picture total area: 7277.091
0	Area black: 7258.1898
Black area	Area yellow: 0
7258.1898	Background (Gray): 18.9012
Yellow + Black area	Area A:
7258.1898	Area B:
Background (Gray)	Area A+B: 0
18.9012	Relation black to yellow+black: 100%
	Relation yellow to yellow+black: 0%
Memory Area B	
M+ M- R	
Memory Area A	
M+ M- R	

Figure 22: Calculation of bubble density for $D_p= 2.36\text{mm}$, 0.25 bar

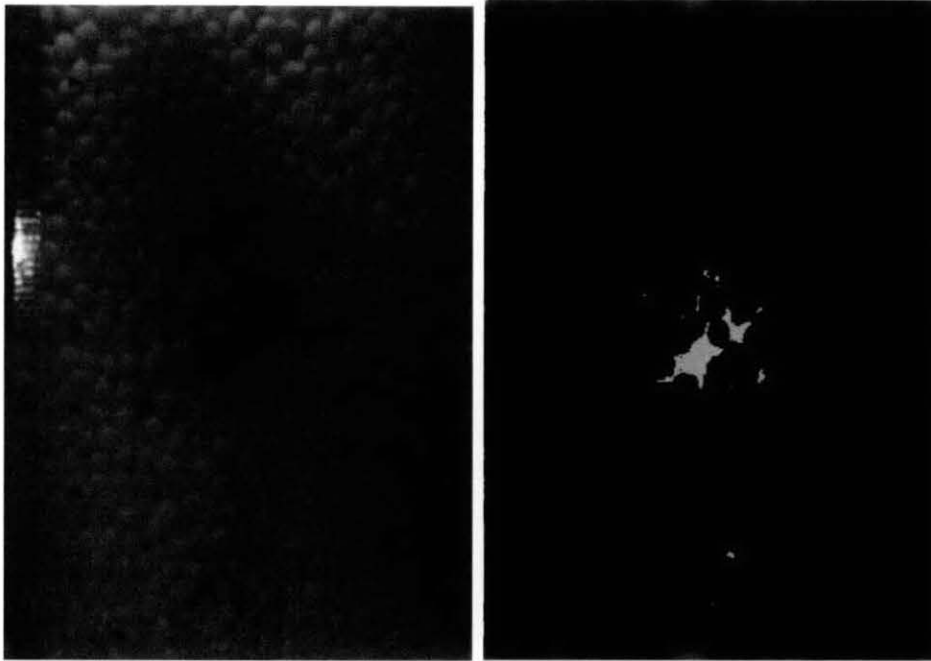


Figure 23: Principle of digital image analysis for a bubble density (a) original image (b) binary image for $D_p = 2.36\text{mm}$, 0.5 bar

All surface area distances are in square mm	
Whole image	
Yellow area	Picture total area: 7401.6986
0	Area black: 7270.3005
Black area	Area yellow: 0
7270.3005	Background (Gray): 131.3981
Yellow + Black area	Area A:
7270.3005	Area B:
Background (Gray)	Area A+B: 0
131.3981	Relation black to yellow+black: 100%
	Relation yellow to yellow+black: 0%
Memory Area B	
<input type="button" value="M+"/> <input type="button" value="M-"/>	<input type="button" value="R"/>
Memory Area A	
<input type="button" value="M+"/> <input type="button" value="M-"/>	<input type="button" value="R"/>

Figure 24: Calculation of bubble density for $D_p = 2.36\text{mm}$, 0.5 bar

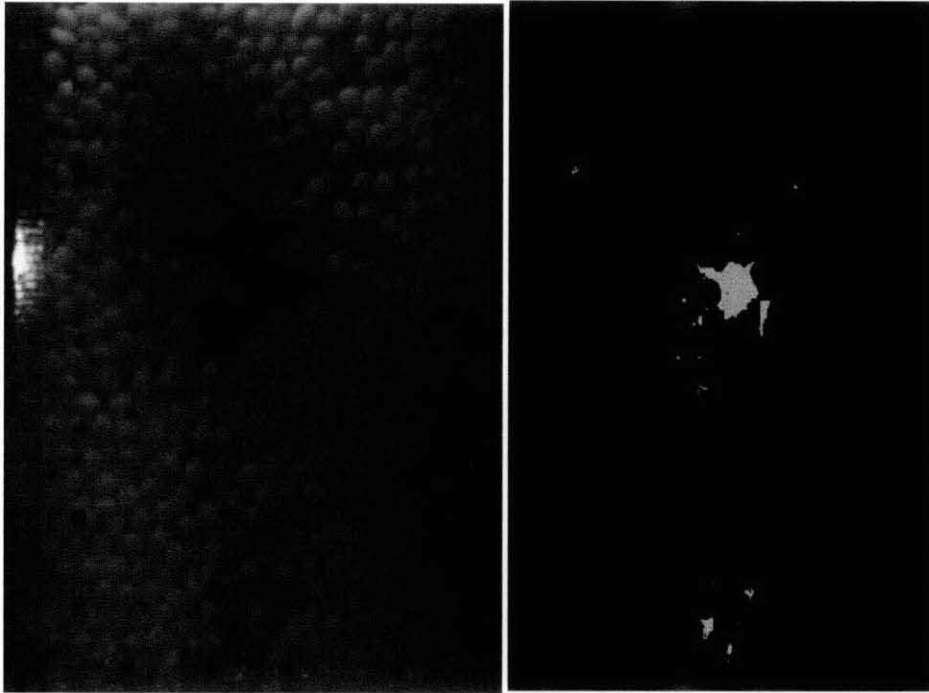


Figure 25: Principle of digital image analysis for a bubble density (a) original image (b) binary image for $D_p = 2.36\text{mm}$, 0.75 bar

All surface area distances are in square mm

Whole image	
Yellow area	Picture total area: 7426.6202
0	Area black: 7361.9362
Black area	Area yellow: 0
7361.9362	Background (Gray): 64.684
Yellow + Black area	Area A:
7361.9362	Area B:
Background (Gray)	Area A+B: 0
64.684	Relation black to yellow+black: 100%
	Relation yellow to yellow+black: 0%
Memory Area B	
<input type="button" value="M+"/> <input type="button" value="M-"/>	<input type="button" value="R"/>
Memory Area A	
<input type="button" value="M+"/> <input type="button" value="M-"/>	<input type="button" value="R"/>

Figure 26: Calculation of bubble density for $D_p = 2.36\text{mm}$, 0.75 bar

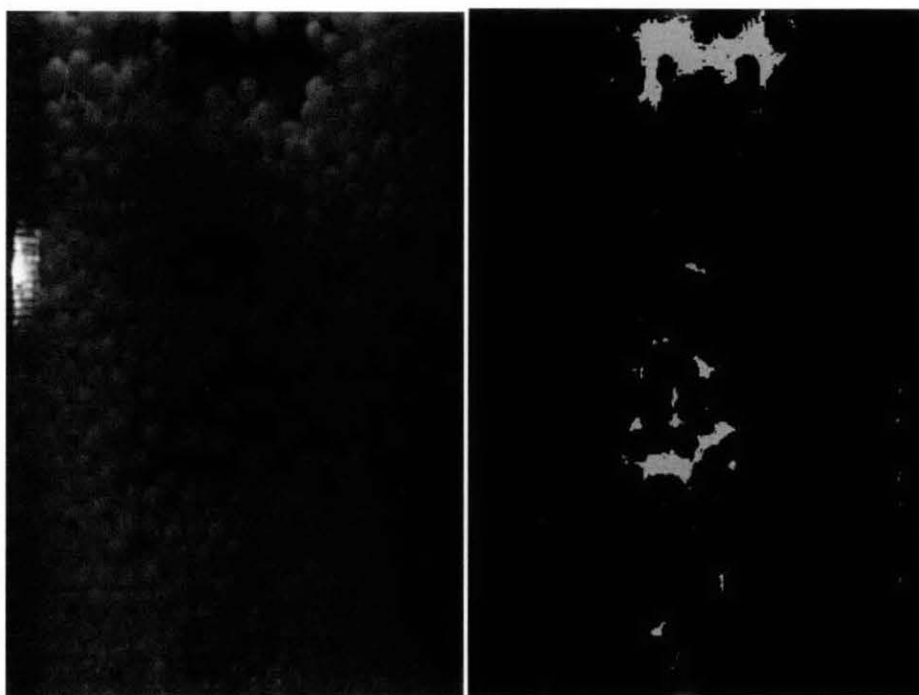


Figure 27: Principle of digital image analysis for a bubble density (a) original image (b) binary image for $D_p= 2.36\text{mm}$, 1.0 bar

All surface area distances are in square mm

Whole image	
Yellow area	Picture total area: 7451.3418
0	Area black: 7253.0795
Black area	Area yellow: 0
7253.0795	Background (Gray): 198.4623
Yellow + Black area	Area A:
7253.0795	Area B:
Background (Gray)	Area A+B: 0
198.4623	Relation black to yellow+black: 100%
	Relation yellow to yellow+black: 0%
Memory Area B	
<input type="button" value="M+"/> <input type="button" value="M-"/>	<input type="button" value="R"/>
Memory Area A	
<input type="button" value="M+"/> <input type="button" value="M-"/>	<input type="button" value="R"/>

Figure 28: Calculation of bubble density for $D_p= 2.36\text{mm}$, 1.0 bar

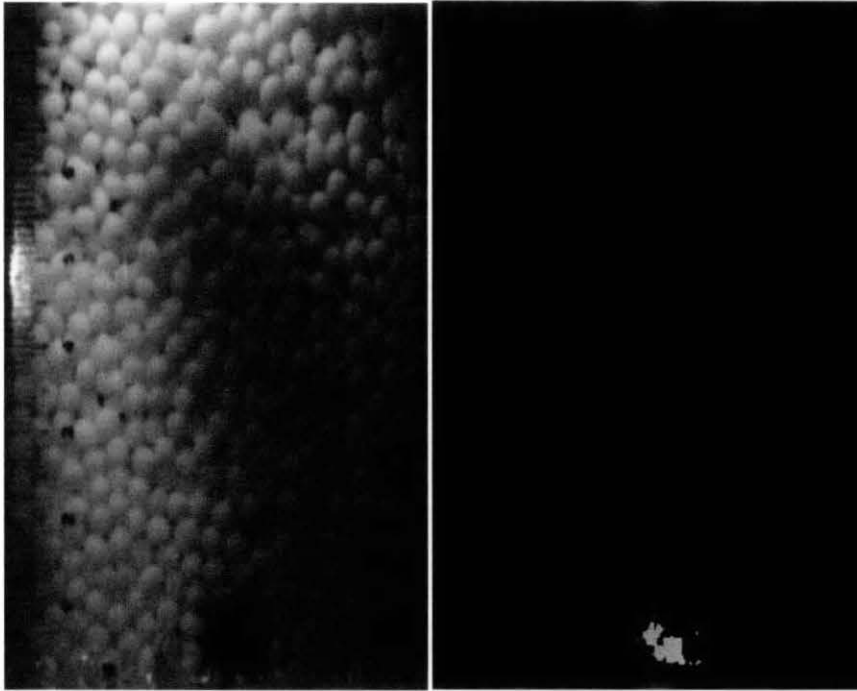


Figure 29: Principle of digital image analysis for a bubble density (a) original image (b) binary image for $D_p= 3.35\text{mm}$, 0.25 bar

All surface area distances are in square mm	
Whole image	
Yellow area	Picture total area: 7406.7589
0	Area black: 7381.4674
Black area	Area yellow: 0
7381.4674	Background (Gray): 24.2915
Yellow + Black area	Area A:
7381.4674	Area B:
Background (Gray)	Area A+B: 0
24.2915	Relation black to yellow+black: 100%
	Relation yellow to yellow+black: 0%
Memory Area B	
<input type="button" value="M+"/> <input type="button" value="M-"/>	<input type="button" value="R"/>
Memory Area A	
<input type="button" value="M+"/> <input type="button" value="M-"/>	<input type="button" value="R"/>

Figure 30: Calculation of bubble density for $D_p= 3.35\text{mm}$, 0.25 bar

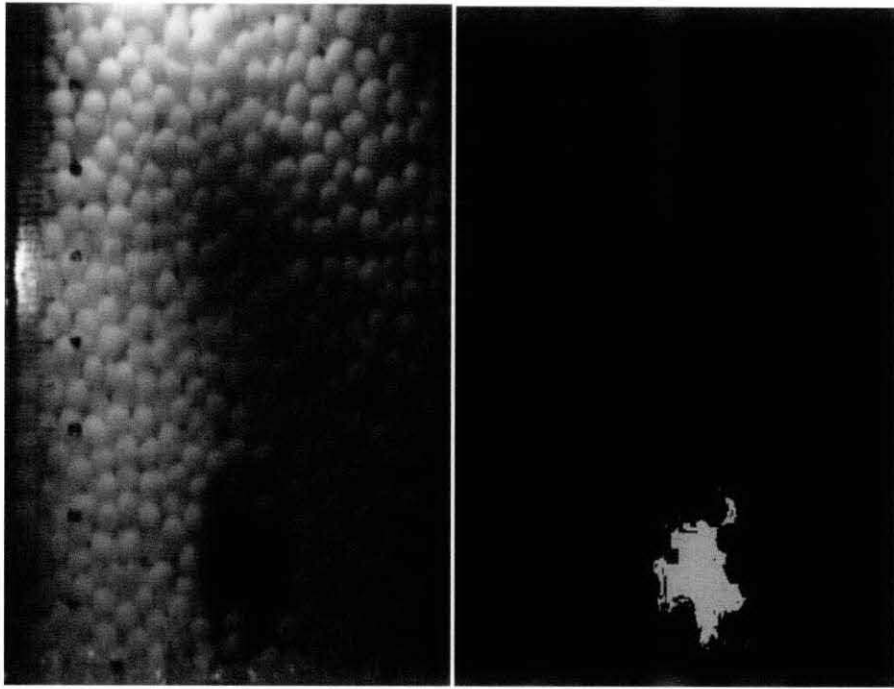


Figure 31: Principle of digital image analysis for a bubble density (a) original image (b) binary image for $D_p = 3.35\text{mm}$, 0.5 bar

All surface area distances are in square mm

Whole image	
Yellow area 0	Picture total area: 7417.0996
Black area 7276.1109	Area black: 7276.1109
Yellow + Black area 7276.1109	Area yellow: 0
Background (Gray) 140.9887	Background (Gray): 140.9887
	Area A:
	Area B:
	Area A+B: 0
	Relation black to yellow+black: 100%
	Relation yellow to yellow+black: 0%
Memory Area B	
M+ M- R	
Memory Area A	
M+ M- R	

Figure 32: Calculation of bubble density for $D_p = 3.35\text{mm}$, 0.5 bar

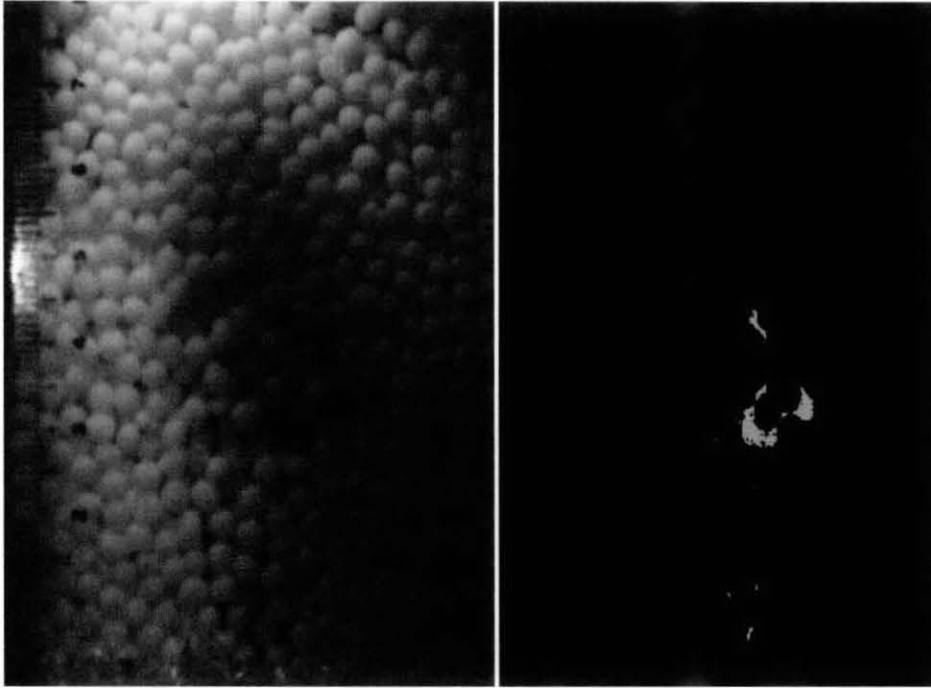


Figure 33: Principle of digital image analysis for a bubble density (a) original image (b) binary image for $D_p= 3.35\text{mm}$, 0.75 bar

All surface area distances are in square mm

Whole image	
Yellow area	Picture total area: 7260.99
0	Area black: 7227.3179
Black area	Area yellow: 0
7227.3179	Background (Gray): 33.6721
Yellow + Black area	Area A:
7227.3179	Area B:
Background (Gray)	Area A+B: 0
33.6721	Relation black to yellow+black: 100%
	Relation yellow to yellow+black: 0%
Memory Area B	
<input type="button" value="M+"/> <input type="button" value="M-"/>	<input type="button" value="R"/>
Memory Area A	
<input type="button" value="M+"/> <input type="button" value="M-"/>	<input type="button" value="R"/>

Figure 34: Calculation of bubble density for $D_p= 3.35\text{mm}$, 0.75 bar

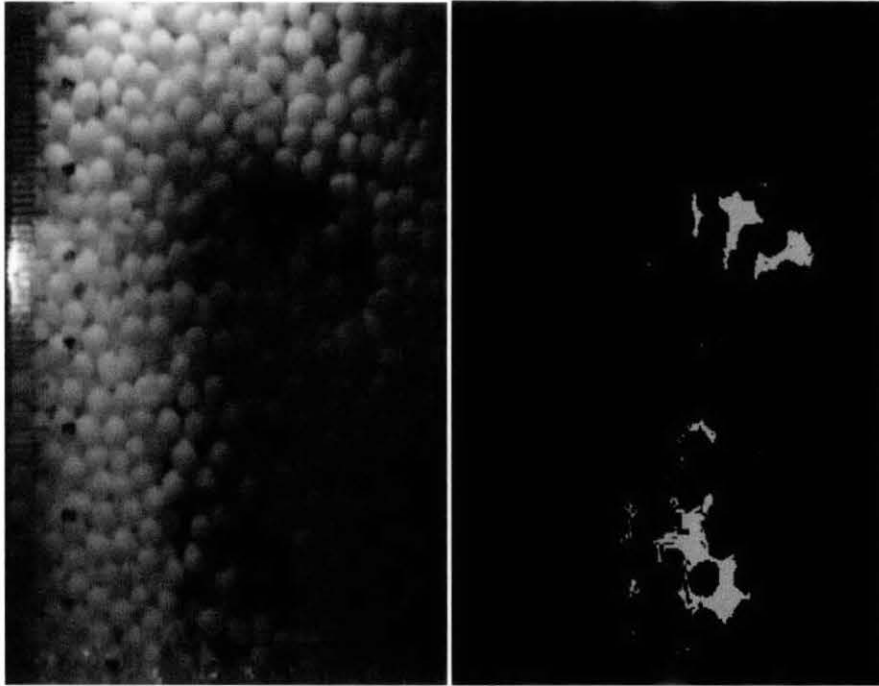


Figure 35: Principle of digital image analysis for a bubble density (a) original image (b) binary image for $D_p= 3.35\text{mm}$, 1.0 bar

All surface area distances are in square mm

Whole image	
Yellow area	Picture total area: 7240.4787
0	Area black: 7079.7487
Black area	Area yellow: 0
7079.7487	Background (Gray): 160.73
Yellow + Black area	Area A:
7079.7487	Area B:
Background (Gray)	Area A+B: 0
160.73	Relation black to yellow+black: 100%
	Relation yellow to yellow+black: 0%
Memory Area B	
M+ M-	R
Memory Area A	
M+ M-	R

Figure 36: Calculation of bubble density for $D_p= 3.35\text{mm}$, 1.0 bar

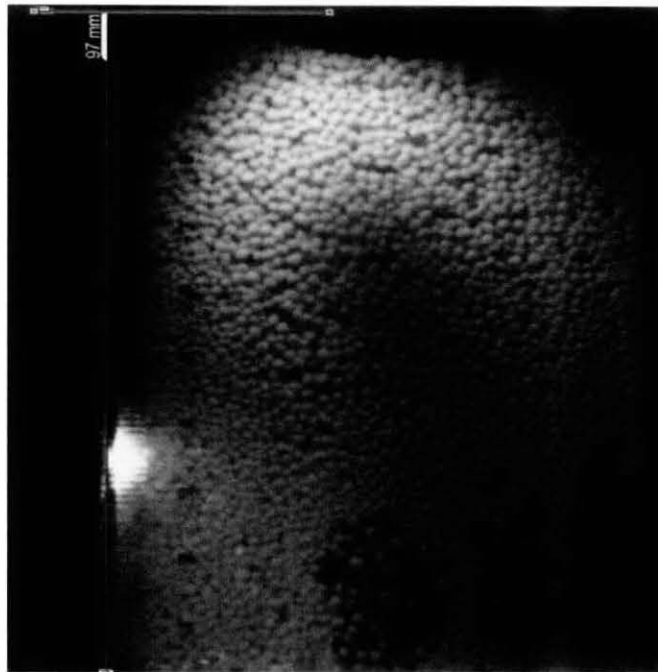
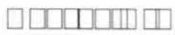


Figure 37: Bed expansion at $D_p = 1.64\text{mm}$, 0.25 bar



Figure 38: Bed expansion at $D_p = 1.64\text{mm}$, 0.5 bar



Figure 39: Bed expansion at $D_p= 1.64\text{mm}$, 0.75 bar

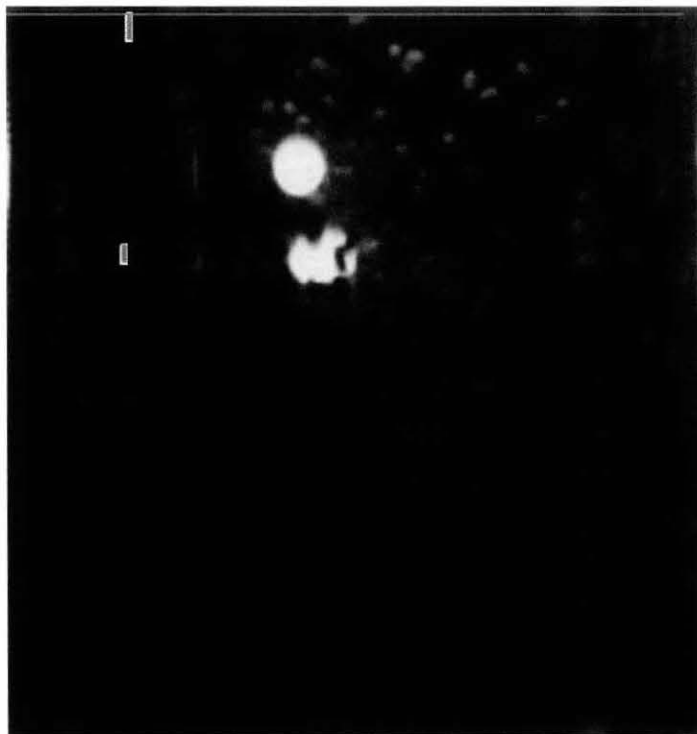


Figure 40: Bed expansion at $D_p= 1.64\text{mm}$, 1.0 bar

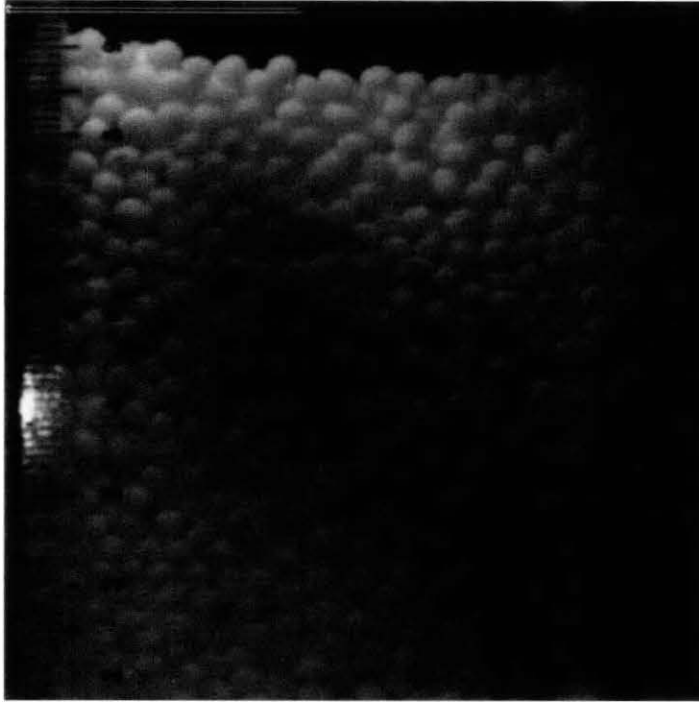


Figure 41: Bed expansion at $D_p = 2.36\text{mm}$, 0.25 bar

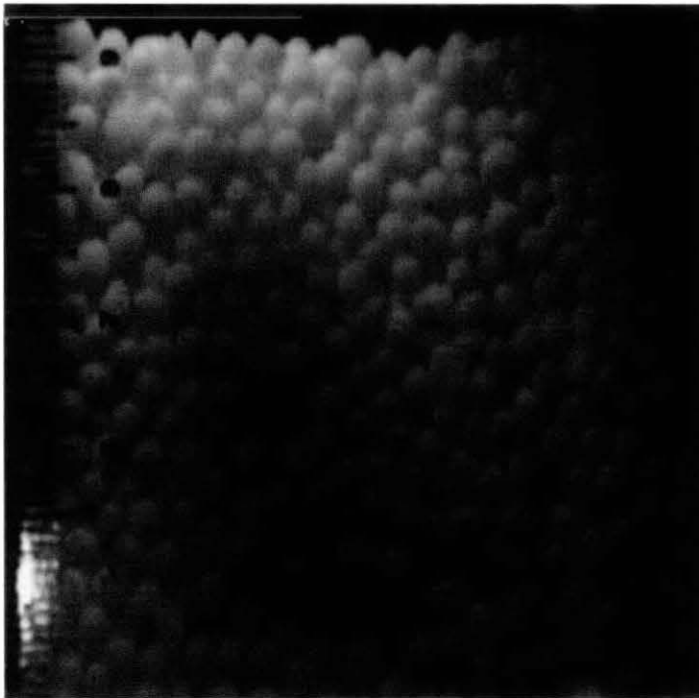


Figure 42: Bed expansion at $D_p = 2.36\text{mm}$, 0.5 bar

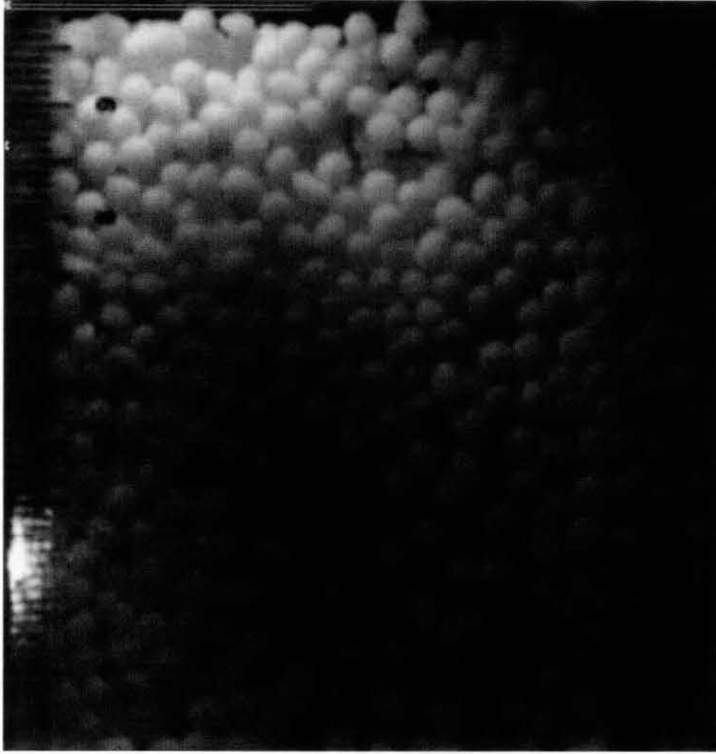


Figure 43: Bed expansion at $D_p= 2.36\text{mm}$, 0.75 bar

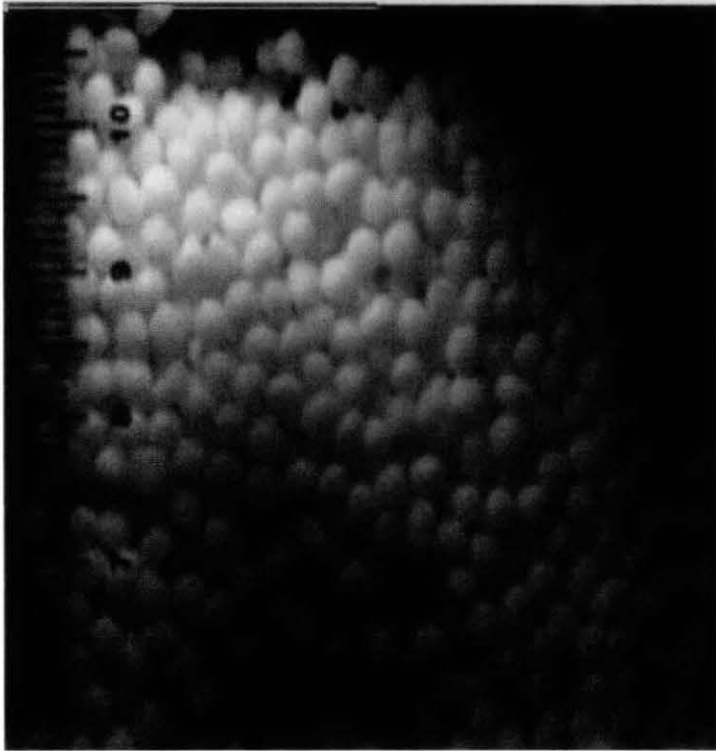


Figure 44: Bed expansion at $D_p= 2.36\text{mm}$, 0.75 bar

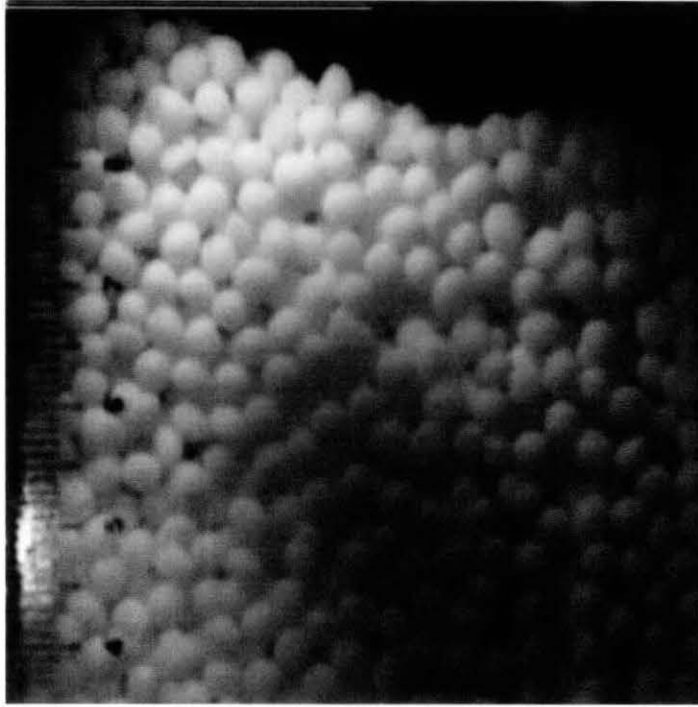


Figure 45: Bed expansion at $D_p= 3.35\text{mm}$, 0.25 bar

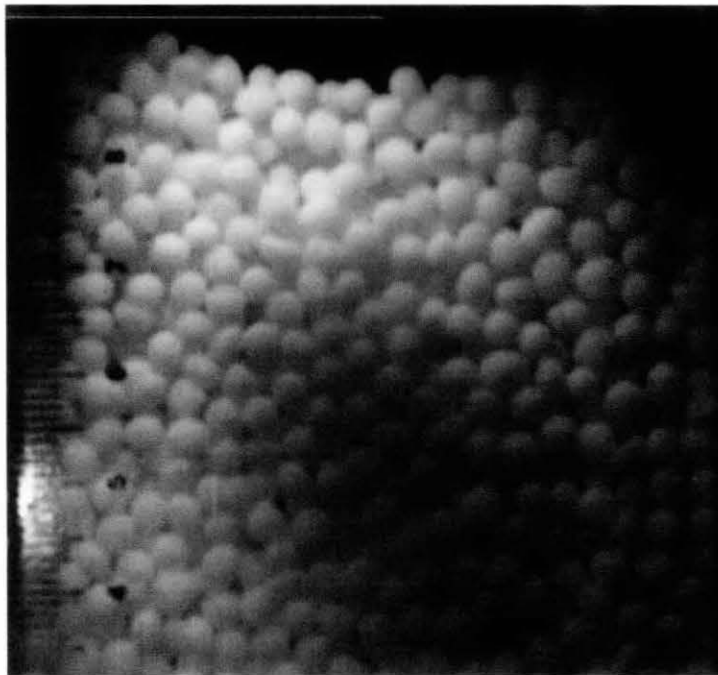


Figure 46: Bed expansion at $D_p= 3.35\text{mm}$, 0.5 bar

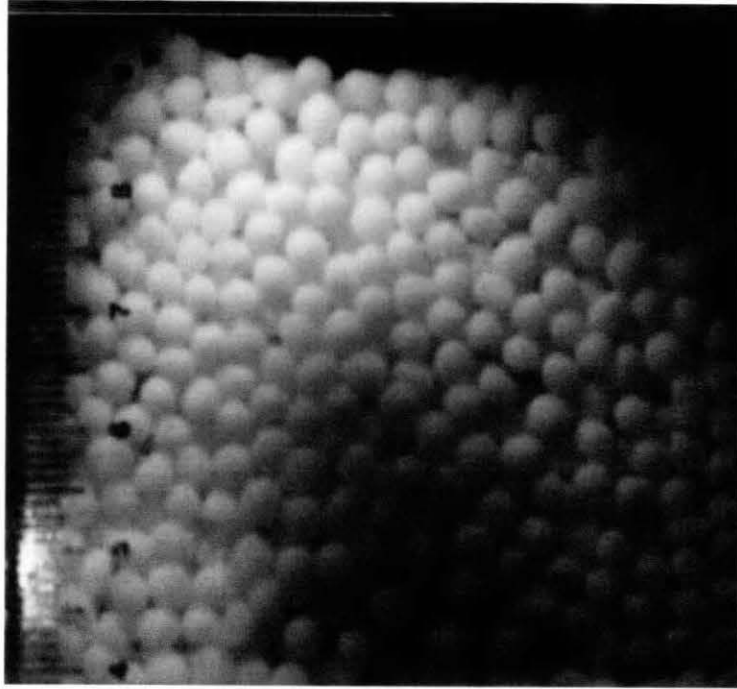


Figure 47: Bed expansion at $D_p= 3.35\text{mm}$, 0.75 bar

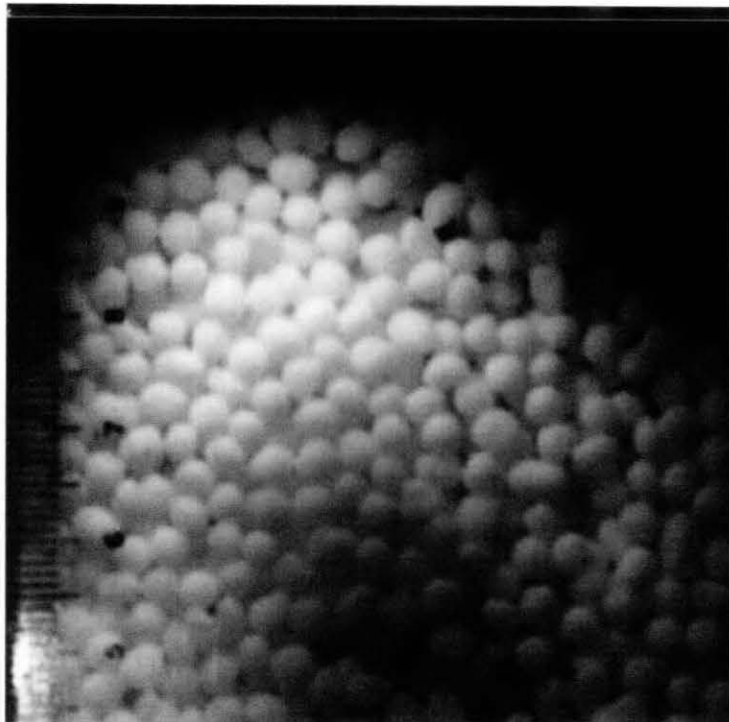


Figure 48: Bed expansion at $D_p= 3.35\text{mm}$, 1.0 bar

□ □ □ □ □ □ □ □ □ □

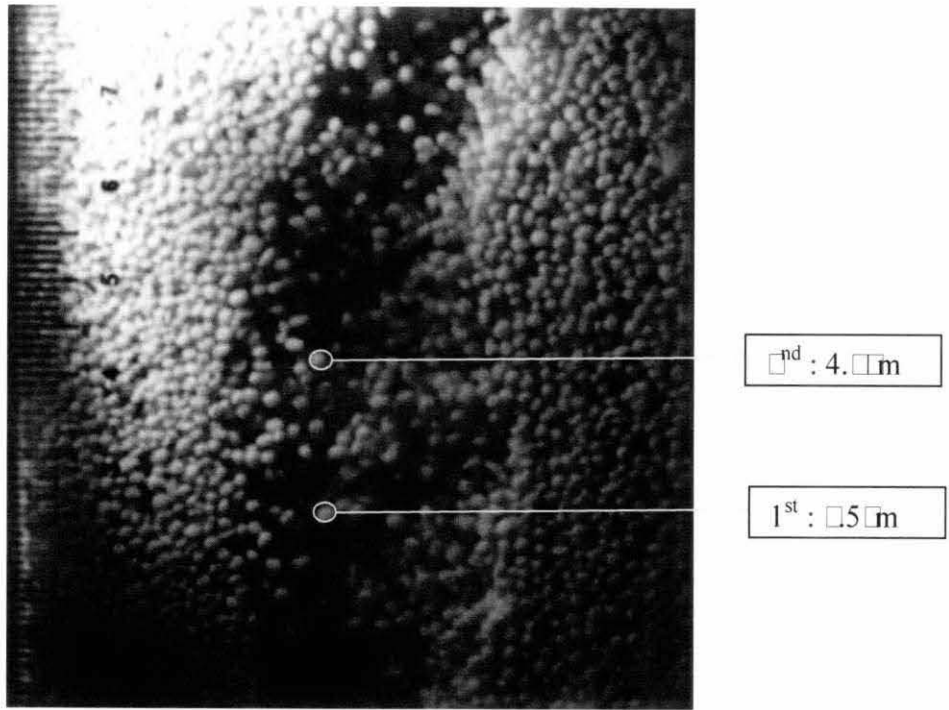


Figure 4: Image at Car point 0100 or $D_p = 1.4$ mm, 0.5 bar

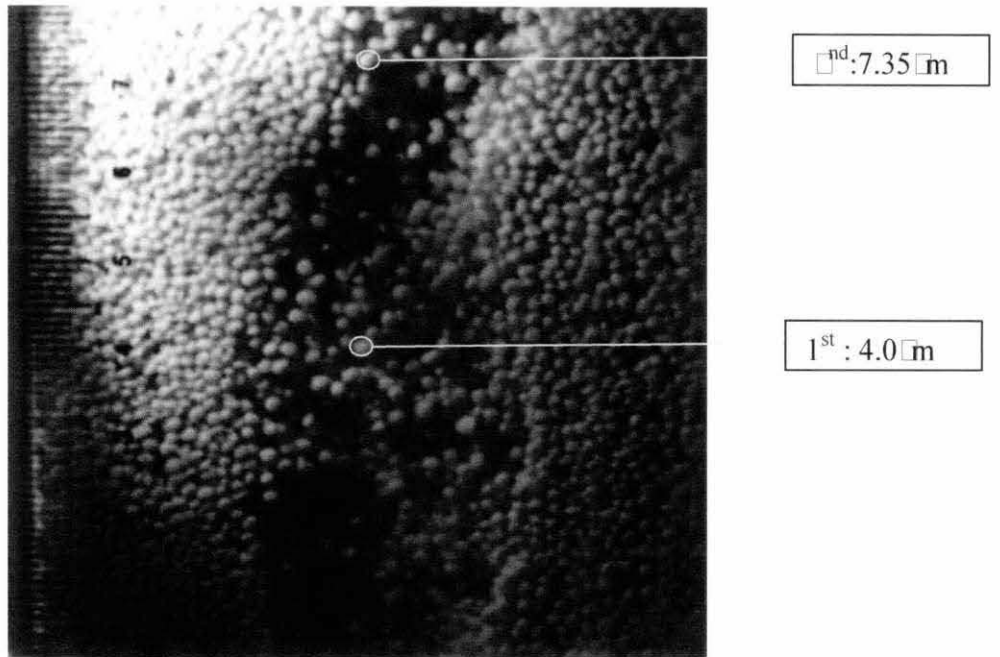


Figure 50: Image at End point 0181 or $D_p = 1.4$ mm, 0.5 bar

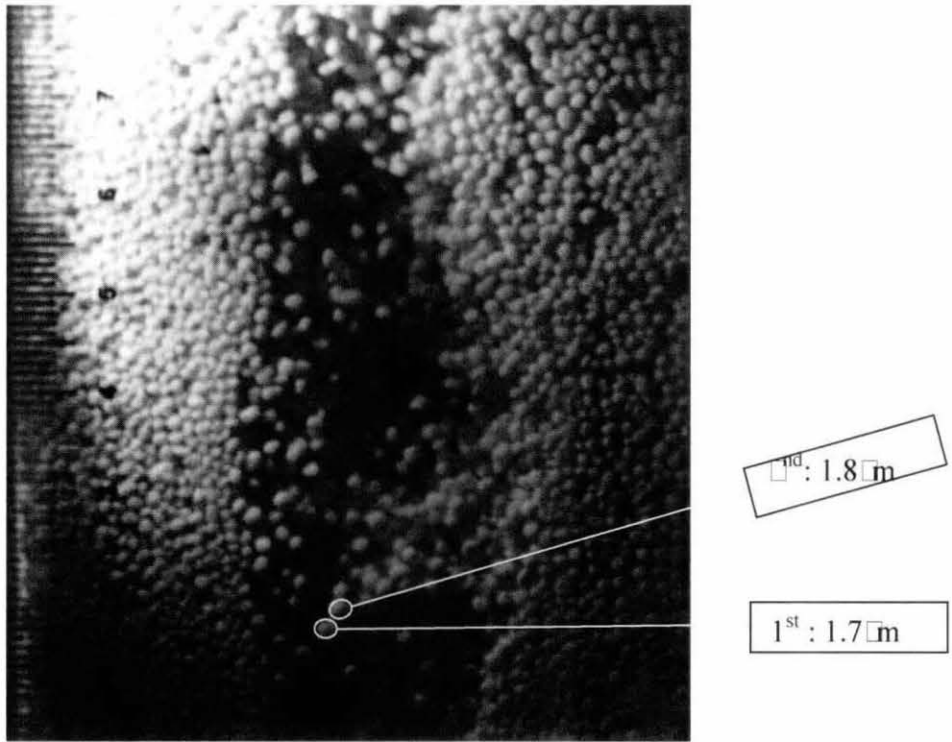


Figure 51: μ graph at start point 007 or $D_p = 1.4 \mu\text{m}$, 0.75 bar

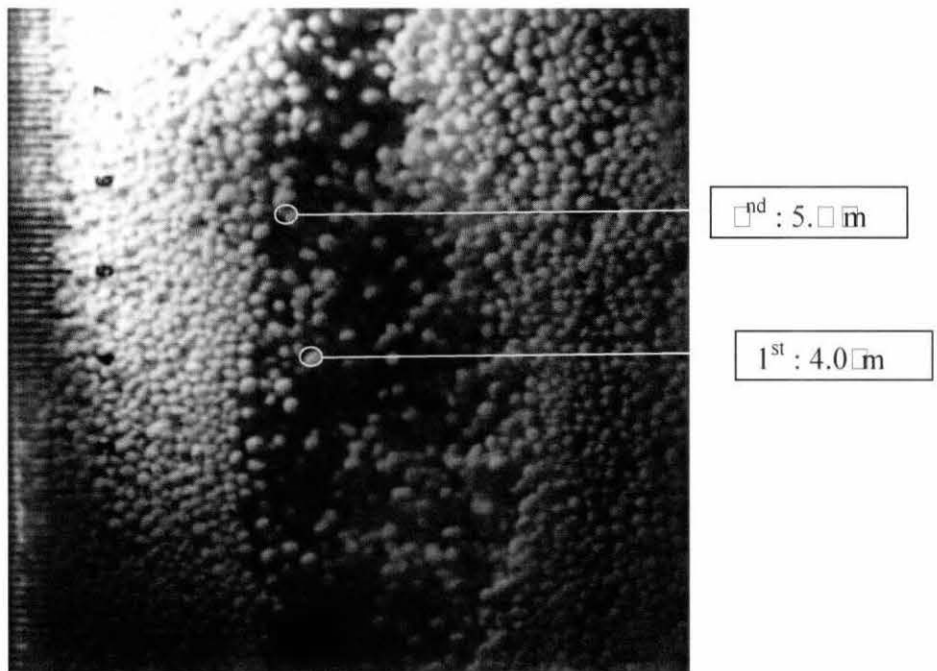


Figure 52: μ graph at end point 0154 or $D_p = 1.4 \mu\text{m}$, 0.75 bar

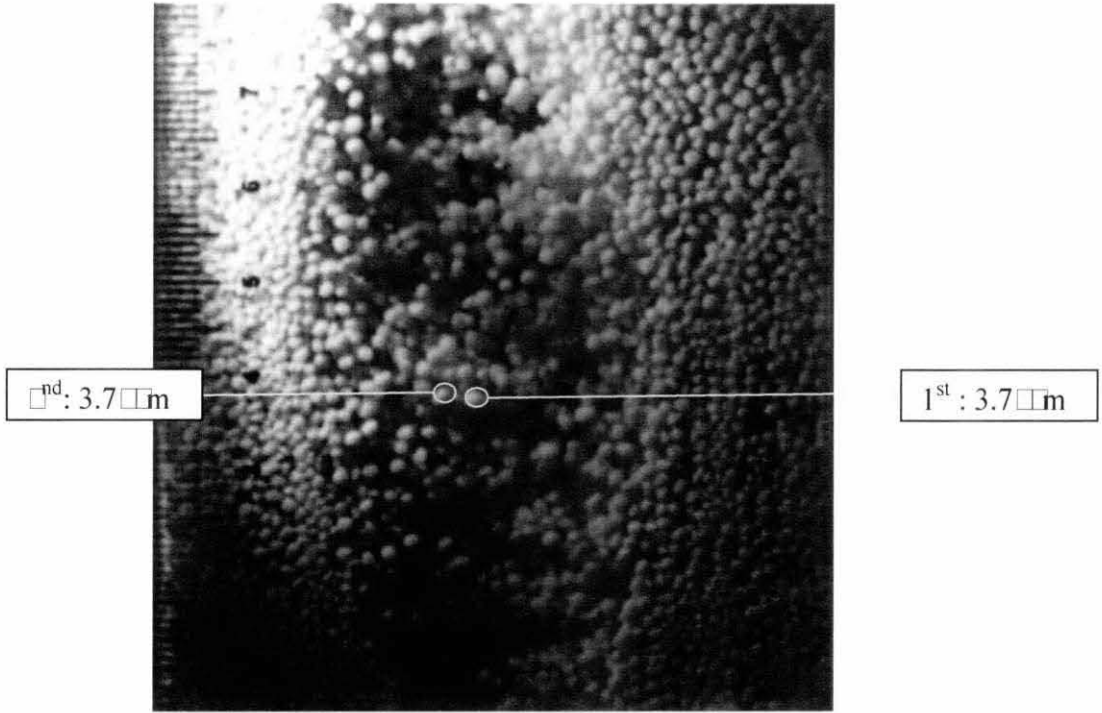


Figure 53: λ_{eff} at λ_{ar} point 0001 or $D_p = 1.4 \text{ mm}$, 1.0 bar

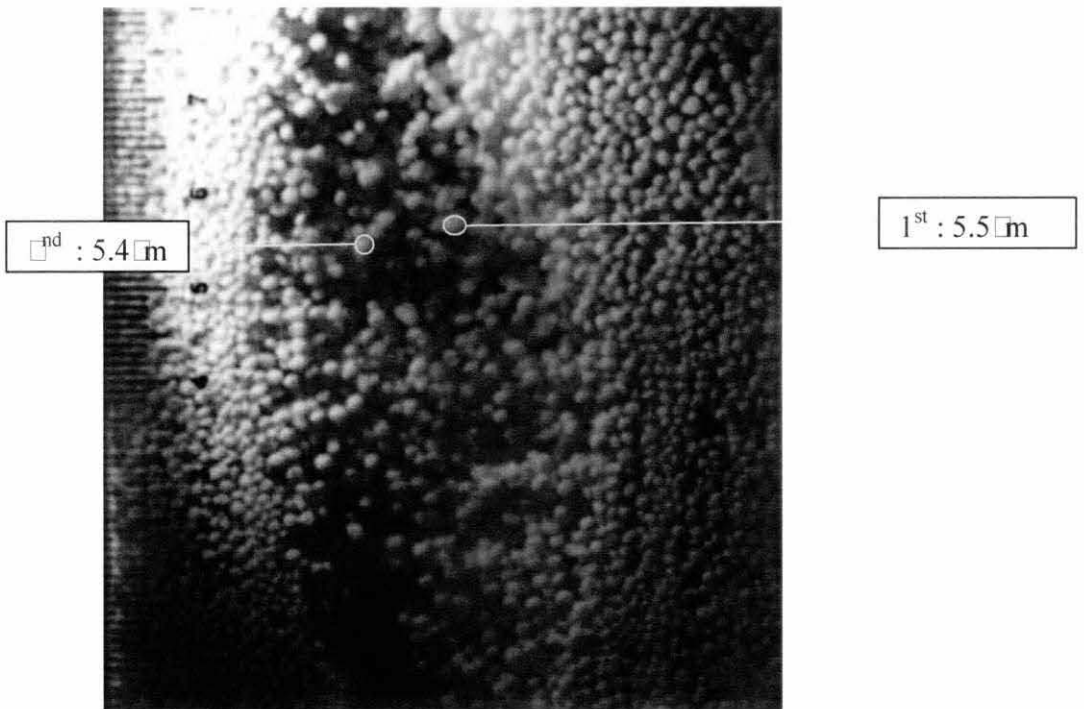


Figure 54: λ_{eff} at λ_{nd} point 0031 or $D_p = 1.4 \text{ mm}$, 1.0 bar